ABSTRACT

Title of thesis	Reliability Assessment of Rolling Piston Rotary Compressors
Degree Candidate	Layla Monajemi
Degree and Year	Master of Science, 2004
Thesis directed by	Professor Reinhard Radermacher, Ph.D. Department of Mechanical Engineering

The performance of a compressor changes during its lifetime, depending on various parameters such as operating conditions, type of the compressor, working fluid and type of the oil being used. Most performance degradation of the compressor is due to wear on the moving mechanical parts inside the compression vessel. Wear develops on the contact point(s) or area(s) between the moving and fixed mechanical parts inside the compressor when there is a lack of lubrication. In a rolling piston rotary compressor, the most vulnerable regions are the vane and roller contact area, and the shaft and journal bearing area. As the amount of wear increases, leakage through the clearances inside the compression compartment increases as well. An increase in the amount of leakage degrades the volumetric efficiency and the overall performance of the compressor.

The objectives of this study are to predict the life span of rolling piston rotary-type compressors through the measurement of wear on the roller under accelerated test conditions, and predict the effect of wear on the degradation of compressor performance. In order to be able to estimate the amount of wear under different operating pressures, a correlation between operating pressures, amount of wear, and degradation of performance was developed. Then the change in compressor performance was estimated using a computer simulation program which takes into account the effect of leakage through the clearances inside the compression vessel based on the operating conditions provided.

One unit of rolling piston rotary type compressor was tested under accelerated operating conditions. An initial increase in the capacity and volumetric efficiency of the compressor was achieved due to aging affects. Then the performance of the compressor started to degrade due to increase in the amount of refrigerant leakage from suction pocket to discharge pocket of the compression compartment.

RELIABLITY ASSESMENT OF ROLLING PISTON ROTARY COMPRESSORS

By

Layla Monajemi

Thesis submitted to the Faculty of the Graduate School of the University of Maryland, College Park in partial fulfillment
of the requirements for the degree of
Master of Science
2004

Advisory Committee:

Professor Reinhard Radermacher, Ph.D., Chairman/Advisor

Professor Mohammad Modarres, Ph.D., Committee Member

Assistant Professor Bao Yang, Ph.D., Committee Member

Dedication

This is lovingly dedicated to my parents and Reza for their endless love, support, and encouragement that made this work possible

Acknowledgement

My thanks and sincere appreciation goes to Dr. Reinhard Radermacher for providing the opportunity to continue my education. Without his wisdom, encouragement, and advice this work would not be completed. I am also very grateful for the support of Dr. Yunho Hwang whose guidance was very helpful to carry on my work.

Special thanks also goes to the Heat Pump Lab team members, both past and present – namely, John Linde, Lorenzo Cremaschi, Reni Muller, Jan Muehlbauer, Hajo Huff, James Kalinger, Xudong Wang, Amr Gado, Jun-Pyo Lee, J.K. Hong, and Aydin Celik. It was a pleasure working with each and every one of you.

Finally, I would like to express my gratitude to my parents, my brother and all my extended family and friends, either here or back home, who supported and trusted me with encouragement, devotion and love.

Table of Contents

List of Figures

List of Tables

1 Introduction

1.1 Overview

The performance of a compressor changes during its lifetime, depending on various parameters such as operating conditions, type of the compressor, working fluid and type of the oil being used. Most performance degradation of the compressor is due to wear on the moving mechanical parts inside the compression vessel. Wear develops on the contact point(s) or area(s) between the moving and fixed mechanical parts inside the compressor when there is a lack of lubrication. In a rolling piston rotary compressor, the most vulnerable regions are the vane and roller contact area, and the shaft and journal bearing area. As the amount of wear increases, leakage through the clearances inside the compression compartment increases as well. An increase in the amount of leakage degrades the volumetric efficiency and the overall performance of the compressor.

The objectives of this study are to predict the life span of rolling piston rotary-type compressors through the measurement of wear on the roller under accelerated test conditions, and predict the effect of wear on the degradation of compressor performance. In order to be able to estimate the amount of wear under different operating pressures, a correlation between operating pressures, amount of wear, and degradation of performance is developed. Then the change in compressor performance is estimated using a computer simulation program which takes into account the effect of leakage through the clearances inside the compression vessel based on the operating conditions provided.

1.2 Motivation

Rolling piston type rotary compressors are widely used in air conditioning unites. They have many advantages over reciprocating type compressors such as small size, light weight, low cost and high performance. However, these advantages are only achieved when the compressor is well designed and assembled. One of the most important factors affecting rolling piston compressor's performance are leakages through clearances [Yanagiswa, 1985]. In this type of compressors, there are many different clearances. The magnitude of each clearance is decided by design and practically kept within a tolerance by the selective matching of parts when a compressor is assembled.

Although there are a lot of compressor models which predicts the performance of the compressor under different conditions, no model is available in open literature that predicts the degradation of compressor performance according to increase in the amount of leakage through internal clearances associated with the amount of wear on the rolling piston.

1.3 Objectives

The focus of this study is on the effect of internal leakage on the performance of rolling piston rotary type compressors. There are different leakage paths inside the compression compartment of a rolling piston rotary type compressor. The amount of refrigerant which leaks from the high pressure pocket to the low pressure pocket depends on the

characteristics of these leakage paths. As the moving parts inside the compression compartment wear out, the clearances between the moving parts increases and as the consequence, refrigerant leakage between the pockets increases. The objective of this study is to understand the effect of roller surface wear out on the amount of refrigerant leakage through the outer diameter of the roller and cylinder wall.

The objectives of this thesis are as follow:

1. Investigation of wear on the rolling piston of a rotary compressor through experiment.
2. Measuring the performance degradation of the compressor over time under accelerated operating conditions through experiment
3. Simulate the amount of wear on the outer diameter of the rolling piston
4. Simulate the performance degradation of the compressor over time as wear increases over time
5. Predict the life span of the compressor at normal use condition
6. Verification of simulation results with experimental data

2 Background

2.1 Literature Review

Although a lot of research has been done on rolling piston rotary type compressors and there are a lot of computer models available for this type of compressors, but the model was not found in open literature which predicts the performance of this type of compressor according to the amount of refrigerant leakage through internal clearances of the compression compartment. Wakabayashi et. al (1982) analyzed the performance of rolling piston rotary type compressors. They studied the effect of different factors on the performance of these types of compressors such as heat transfer through the shell. Yanagiswa (1982) analyzed the motion of the rolling piston and the friction coefficient at the roller and vane interface. Fujimoto et. al (1984) carried out a tribological analysis on rolling piston rotary type compressor involving the temperature calculation at the roller and vane interface, and effective lubrication in the cold start and defrosting cycles of the refrigerator. Takebayashi et. al (1998) developed a new method to accelerate the estimation of wear in rolling piston type rotary compressors. Davis and Cusano (1992) conducted an extensive study on friction and wear characteristics of compressor contacts lubricated by different oil-refrigerant mixtures. Also Jenkins (1998) developed a detailed model to simulate the performance of rolling piston rotary type compressors under different operating conditions. Although he has mentioned the importance of studying the amount of wear especially on the outer diameter of the rolling piston, but his program doesn't take this factor into account.

2.2 Refrigeration and Air-conditioning

Air-conditioning and refrigeration play an important role in our everyday life. Air-conditioning systems exist in our offices, homes, personal automobiles, buses, airplanes and almost every closed environment that we deal with on daily basis. Refrigeration systems are extensively used in food industry as well as many other industries such as gas separation, natural gas liquefaction, and ice production.

The most commonly used method in air-conditioning and refrigeration industry is the vapor compression cycle. Vapor compression cycles have many complex variations, but basically a vapor compression cycle consists of four main components which are compressor, evaporator, condenser, and expansion valve. In vapor compression cycle, vapor refrigerant which is assumed to be saturated or superheated vapor is compressed in an isentropic compression process until condensing pressure is reached. The hot and superheated gas enters the condenser. In condenser, the hot gas rejects heat to its surrounding environment (heating effect) during a constant pressure process until saturated liquid condition is reached. Then, the refrigerant expands through a throttling valve, where partial evaporation occurs as the pressure drops across the valve. As the result of throttling process, low pressure saturated liquid can evaporate at low pressure in the evaporator and produce cooling effect.

2.3 Compressors

Compressors are mechanically the most complex and often the most expensive part of the cycle. Compressors can be divided into two major categories; positive displacement and dynamic. Positive displacement compressors, increase the pressure of the vapor refrigerant by decreasing the volume. Examples are the reciprocating, rotary (rolling piston, rotary vane, single screw, and twin screw), and scroll. Dynamic compressors increase the pressure of the vapor refrigerant by transferring of angular momentum from the rotating member to the vapor continuously.

2.4 Rolling Piston Rotary Type Compressor

Rolling piston, or fixed vane, rotary compressors are used in household refrigerators and air-conditioning units in sizes up to about 3 hp [ASHRAE Handbook, Chapter 34, pp. 9-11]. This type of compressor uses roller mounted on the eccentric of a shaft with single vane positioned in the non-rotating cylindrical housing which is called the cylinder block. The vane reciprocates in a slot which is machined in the cylinder block. This reciprocation motion is caused by the eccentrically moving rolling piston. Figure 1 shows the mechanism and the structure of the compression vessel.

The fluid is contained in the volume between the piston, vane, and cylinder wall. As the piston roles over the inlet port, a pocket is formed between the right side of the vane, the lower right side of the cylinder wall and the lower right side of the piston. As the piston continues its course, the chamber volume increases and fluid enters the pocket. In a

compressor application the inlet port stays open for one complete rotation of the piston along the inner wall of the cylinder. This volume is referred to as suction chamber [Figure 3]. As the piston roles over the inlet port again, the fluid in the chamber is sealed from the inlet reservoir and suction chamber is transformed into discharge chamber. In the further course of the rotation, the fluid in discharge chamber is compressed and, when the pressure reaches discharge level, expelled from the compressor. As the piston moves over the discharge port a small amount of fluid remains in the clearance volume. It undergoes sudden expansion, as the piston opens the clearance volume to the next chamber, which is still at inlet pressure.

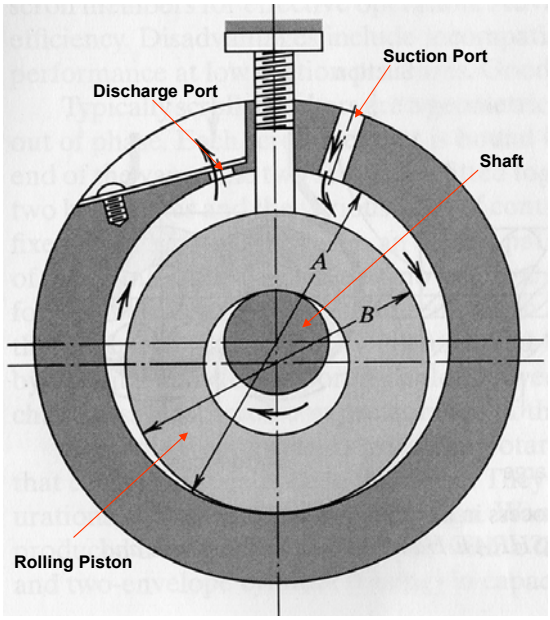

Figure 1: Rolling Piston Rotary Type Compression Mechanism [ASHRAE Handbook, 2000 [34.9]]

Displacement for this compressor can be calculated from:

$$V_d = \frac{\pi \times H \times (A^2 - B^2)}{4} \qquad \text{Equation 1}$$

where

V_d = displacement

H = cylinder block height

A = cylinder diameter

B = roller diameter

The motor, stator, and compressor are mounted in the compressor housing. This feature is possible due to low vibration of rotary type compressors, but in reciprocating type compressors the housing and the compressor parts are separated by spring.

Suction gas is directly piped into the suction port of the compressor, and the compressed gas is discharged into the compressor housing shell. This high-side shell design is used because of the simplicity of its lubrication system and the absence of oiling and compressor cooling problems. Compressor performance is also improved because this arrangement minimizes heat transfer to the suction gas and reduces gas leakage area.

The main components of a rotary compressor mechanism consist of a cylinder, a shaft, and an eccentric on the shaft, a roller, two bearings plates and a vane. Among all these components, the moving parts are the shaft, the roller, and the vane. The vane divides the

cylinder room into two different pockets; a compression pocket or so called high pressure pocket and a suction pocket or so called a low pressure pocket. The vane is supported by the spring while its tip end is kept in continues contact with the roller. The vane is always in line contact with the roller by the spring force and the discharge pressure behind the vane; although over time this may turn into a surface contact. Figure 2 shows the structure inside the hermetic case of a rolling piston type rotary compressor.

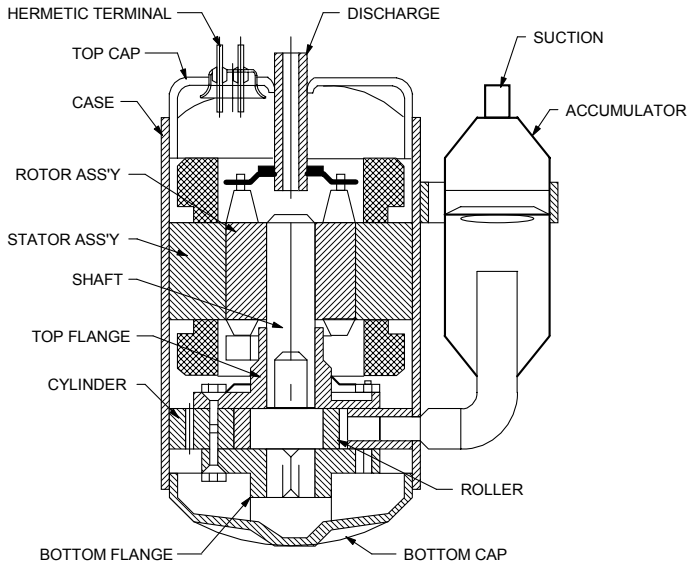

Figure 2: Structure of Rolling Piston Rotary Type Compressor

2.5 Leak Types in Rolling Piston Rotary Type Compressors

Positive displacement mechanisms are characterized by the change of the volume confined by the walls of the compression/expansion chamber. The chamber walls in vapor compression applications are usually made from rigid material. For the volume to be changed, the chamber walls must change position relative to one another. Leakage generally occurs at all moving interfaces. The leak types in most positive displacement devices can be grouped in the following categories:

- Tip leak:

  Approximately rectangular flow channel with approximately constant cross sectional area along the leak path. Example: Between piston and cylinder wall in reciprocating piston mechanism.

- Flank leak:

  Approximately rectangular flow channel with variable cross sectional area along the leak path. Example: Between piston and cylinder wall in rotary piston mechanism.

Some or all of the dimensions of an individual leak path can vary during the compression and processes in the device. The pressure in the reservoir that a leak connects the chamber with may also change during the course of the working cycle of the device (Huff, 2003).

In modeling of the compression process of rolling piston rotary type compressor, the internal leakage requires special attention since the wear on the vane, roller, piston, cylinder, and bearing would affect it. The leaks are characterized by the individual leak paths, containing information about the topology of the device, and by the individual leak types, determining the leakage mechanism. Internal leakage reduces the mass flow rate of the compressor which ultimately reduces cooling capacity of the entire system (Schein, 1998). There are five major leak paths, which are indicated in Figure 1. The leaks across the piston wall and the vane occur on the top and bottom of the device. Since the internal leakages affect the performance of the compressor, their effect has been taken into account in the computer simulation program.

Each leak path is characterized by three dimensions: length, width, and height. Among these three dimensions the effect of wear on the length of the leak path 1 was the main focus in this study.

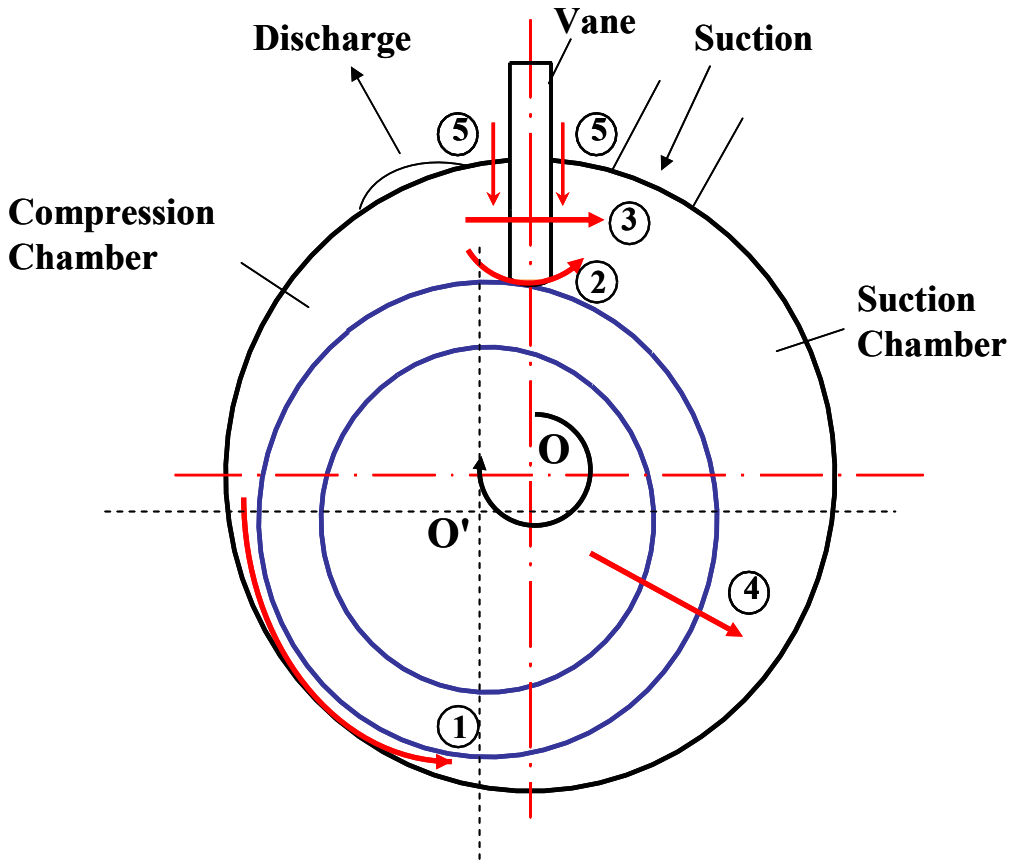

Figure 3: Leakage Paths inside the Rolling Piston Rotary Type Compressor

3 Experimental Setup and Test Procedure

3.1 Test Facility

In order to measure the performance degradation of the rolling piston rotary type compressor over time, a bolted case rotary type compressor which uses R-22 as its working fluid was installed and tested in a vapor compression cycle. The vapor compression cycle was designed and constructed for testing small size compressors with air-conditioning application.

Figure 4 shows the schematic of the test facility. The test stand is equipped with regular four-cycle components which are evaporator, condenser, compressor, and expansion valve. Three are three additional components in the system, which are hot gas bypass valve, filter, and electric suction heater. Hot gas bypass line was installed to have more flexibility in achieving test conditions. To achieve a stable mass flow rate reading, the mass flow meter was installed at the condenser outlet where the refrigerant has the highest density in the cycle. Since the use of the hot gas will deviate both the mass flow rate and enthalpy entering to the evaporator from those measured at the condenser outlet, the refrigerant mass flow rate and enthalpy entering the evaporator would be unknown. Therefore, in case that hot gas bypass is being used, the position of the mass flow meter will be changed to the suction line. The suction filter removes any dirt and moisture in the cycle. The electric heater provides additional heat to ensure the suction gas to be superheated gas. As it is shown in the picture the compressor is housed in an environmental chamber which can provide stable environmental temperature up to 60°C.

Relative humidity and temperature of the chamber can be controlled through the control unit at the front of the chamber.

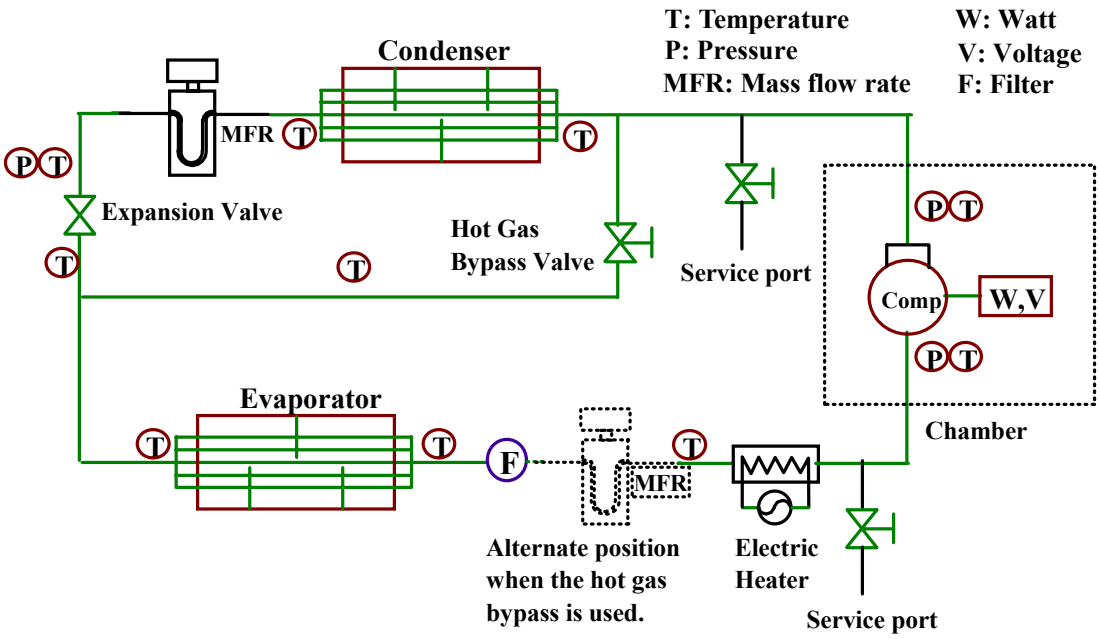

Figure 4: Schematic Drawing of the Experimental Setup

There are two fans installed in front of the evaporator and condenser. The fans are utilized to achieve the desired test conditions and they can be controlled through the data acquisition system. Table 1 presents the specifications of the components of the cycle.

Compressor performance characteristics were measured by various instruments as following.

- Compressor discharge and suction pressures (Pd, Ps) by pressure transducers
- Power consumption by watt meter

- Temperatures (inlet, outlet, accumulator bottom, shell top & bottom) by thermocouples
- Compressor motor RPM by piezoelectric accelerometer

From the measured data, the following characteristics of the compressor were evaluated:

- Cooling capacity
- Compressor power input
- Coefficients of performance
- Refrigerant mass flow rate
- Temperature and pressure at the compressor inlet and outlet
- Sub cooling and superheating
- Volumetric and compression efficiency

Table 1: Component Specifications of the Compressor Test Stand

Components		Manufacture	Description
1	Compressor	Samsung	Model No.=124 HX, 44B Frame Type=Rolling Piston Rotary Type; HCFC R-22, 60 Hz, 1-Phase, 115 V; Evap. Temp. Range: -10°C to 12°C Cond Temp. Range: 28°C to 65°C Max compression ratio: 6 Displacement: 17.64 cc/rev Oil Type: SUNISO-4GSD Initial Charge: 300 cc Net Weight (Including Oil): 11.0 kg Motor Type: Permanent Split Capacitor
2	Environmental Chamber	Barnstead International	Model No.= 702ASDH Capacity= 32.5 Cu.ft Electrical Specifications = 120 V, 60 Hz, 1 phase Refrigerant= HCFC 22 Max Current = 30 Amp Temperature Range= 5 – 60 ° C
3	Condenser	Generic	Type: 1 pass of inlet and outlet Cross Flow, Fin and Tube Heat exchanger Inlet Tube O.D.= 3/8” Outlet Tube O.D = 3/8”
4	Mass Flow Meter	Micromotion	Type: Coriolis Mass Flow Meter Model: CMF025M31NU Mass Flow rate: 1 – 60 g/s Temperature Range= -240 – 240 °C Max Pressure = 850 psi

5	Expansion Device	Swagelok	3/8” O.D. Integral Bonnet Needle Valves Model: SS-1RS6
6	Evaporator	Generic	Type: Fin and Tube Heat Exchanger Fan: Pipe O.D. Inlet = 3/8”; Pipe O.D. Outlet = ¾” Face Area ≈ 3.56 Sq ft
7	Tape Heater	HTS/Amptek Company	Model: AWH-051-060D Max Temp.: 760 °C Watts: 468 Volts: 120 Current: 3.9 Amp
8	Filter Dryer	Sporlan Valve Company	Type: Catch ALL C 464 Function: Moisture Absorber and Filtering Capacity Inlet Tube O.D.: ½” Outlet Tube O.D.: ½”

3.2 Measurements and Data Acquisition System

About 25 sensors were distributed along the system to measure pressures, temperature, flow rates, power consumptions. All the sensors were connected to a Hewlett Packard (HP) 3497A data acquisition and control unit and they are displayed in real time by Quick Basic software program interface.

3.2.1 Temperature and Pressure Measurements

Thermocouples were used to measure temperature at several locations in the test facility. The data acquisition system uses hardware and software compensation to simulate the reference junction, therefore eliminating the need for physical reference junction at constant reference temperature. The voltages from the thermocouples are converted into temperature values using appropriate correlations in the data acquisition program (Hewlett Packard, 1987). Table 2 shows the detailed specifications of the thermocouples.

Absolute pressure transducers are installed at the compressor discharge, compressor suction, and expansion valve inlet. They were Setra Model 280E. Detailed specifications are shown in Table 3. The pressure transducers which were installed at the compressor discharge and expansion valve inlet have the same operating ranges but the one which is installed at the compressor suction has a smaller range which is 0-500 psi.

3.2.2 Mass Flow Rate Measurements

One Coriolis mass flow meter was used to measure the refrigerant mass flow rates. The refrigerant mass flow meter was installed at the condenser outlet. Since the mass flow meter does not provide reliable measurements for two-phase flows, a minimum degree of sub-cooling of about five degrees is necessary to guarantee always one-phase liquid flow through the instrument. The refrigerant mass flow meter specifications are shown in Table 4.

3.2.3 Frequency Measurement

One accelerometer was used to measure the frequency of rotation of the shaft. The accelerometer is magnetic and sticks to the shell of the compressor. Accelerometer together with a power supply is connected to a frequency measurement device which reads and shows the value of the frequency. The accelerometer, coupler, and frequency meter specifications are shown in Table 5.

3.2.4 Power and Voltage Measurement

In order to be able to calculate the efficiency of the compressor, power consumption of the compressor has to be measured. To meet this purpose a power transducer was installed in the system.

Also, to make sure that the compressor does not draw extra current, the line voltage of the compressor was measured. A voltage transducer was also installed in the system to

measure the line voltage. Tables 6 and 7 show the specifications of the power and voltage transducer.

Table 2: Specifications of Thermocouples

Item	Specification
Thermocouple type	T-type
Alloy Combination	Copper-Constantan
Temperature range	-270 to 400 ºC
Accuracy	± 0.5 ºC
Manufacturer	Omega Engineering, Inc.

Table 3: Specifications of Pressure Transducers

Item	Specification
Model	280E
Pressure Range	0-1000 psia and 0-500 psia
Accuracy	± 0.11 % Full Scale
Output	0-5 VDC
Excitation	24 VDC Nominal
Manufacturer	Setra System, Inc.

Table 4: Specifications of the Refrigerant Mass Flow Meter

Item	Specification
Sensor Model	DH025S119SU
Transmitter Model	1700C11ABUEZZZ
Type of Sensor	Coriolis Mass Flow Meter
Flow Range	1 – 60 g/s (≈ 8 – 794 lbs/hr)
Accuracy	± 0.5 % of rate
Maximum Operating Pressure	3000 psig (20.7 MPa)
Maximum Operating Temperature	150 ºC
Output	4 to 20 mA
Manufacturer	Micro Motion Inc.

Table 5: Specifications of the Accelerometer, Coupler, and Digital Multimeter

Item	Digital Multimeter
Model	7552
Manufacturer	Yokogawa
Measurement Range	DC 1000V, AC 700V, DC/AC: 20A
Item	K-Shear Accelerometer
Model	8702B50
SN	2008774
Manufacturer	Kistler
Item	Power Supply/ Coupler
Model	5114
Manufacturer	Kistler

Table 6: Specifications of the Power Transducer

Item	Power Transducer
Model	GH-019D/10K
Current Rating	0-20
Voltage Rating	0-150
Accuracy	0.2% RDG
System	Single-phase
Manufacturer	Ohio Semitronics

Table 7: Specifications of the Voltage Transducer

Item	Voltage Transducer
Model	VT-240A
Voltage Rating	0-300
Accuracy	0.25%
Output	0-1mA Self-powered
System	Single-phase
AC/DC	AC
Manufacturer	Ohio Semitronics

3.3 Test Procedure

As it was described in section 3.2 a bolted case rotary type rolling piston type compressor which uses R-22 as refrigerant was tested in this project as shown in Figure 5. The compressor was a brand new unit.

Figure 5: 44B Samsung Bolted Case Rotary Type Compressor

Before testing, the compressor was disassembled and the outer diameter of the rolling piston in the compression compartment was measured with a digital height measurement device as shown in Figure 6. The height measurement device has the accuracy up to

1 μm . The outer diameter of the roller before testing was measured to be 37.981 mm. Diameter was measured at twenty different points along the outer surface of the rolling piston to minimize error in measurement.

Figure 6: Digital Height Meter

After measurement, the compressor was assembled again and was installed in the test stand. The compressor was continuously tested under specific test condition which is shown in summarized in Table 8 for 30 days.

Table 8: Test Condition

Test	Test B
Discharge Pressure (MPa)	3.38
Suction Pressure (MPa)	0.76
Condensing Temp (°C)	75.9
Evaporating Temp (°C)	13.7

Data was collected for 30 days in order to calculate the volumetric and compression efficiencies over the test period. Volumetric and compression efficiencies are calculated using Equations 2 & 4.

$$e_{vol} = \frac{\dot{m}_{measured}}{\dot{m}_{\max}} \qquad \text{Equation 2}$$

where e_{vol} is the volumetric efficiency, $\dot{m}_{measured}$ is the mass flow rate which is measured by the mass flow meter, and $\dot{m}_{\max}$ is the maximum possible mass flow rate that the compressor can handle which can be calculated using Equation 2.

$$\dot{m}_{\max} = Disp \cdot (RPM / 60) \cdot Den_{suc} \qquad \text{Equation 3}$$

where Disp is the displacement volume of the compressor and Den_{suc} is the density of the refrigerant at the suction of the compressor.

$$e_{comp} = \frac{\dot{m}(h_{dis-s} - h_{suc})}{W_{elec}}$$ Equation 4

where e_{comp} is the compression efficiency, $\dot{m}$ is the measured mass flow rate, h_{dis-s} is the isentropic enthalpy at discharge and h_{suc} is enthalpy at suction.

It is very important to notice that the level of oil in the compressor needs to be kept constant during the test. There is sight glass installed on the shell of the compressor which the level of oil was monitored from.

4 Compressor Simulation

In order to evaluate compressor's performance degradation due to wear on the outer diameter of the rolling piston at different operating conditions, a computer simulation tool has been developed. The program consists of two parts, thermodynamic simulation and wear simulation.

The thermodynamic part simulates the process that the fluid undergoes in a rolling piston rotary type compressor while it is being compressed as it enters the compressor from the suction port till it leaves the compression compartment from the discharge port. A general "Expander and Compressor Simulation" tool was developed as a part of ARTI-21CR project [Huff, 2003]. The simulation takes into account the irreversible processes of valve losses, internal leakage and internal heat transfer. The simulation tool was modified to match the specific characteristics of rolling piston rotary type compressor such as sudden expansion/compression in the discharge valve clearance.

The wear model simulates the amount of wear which occurs on the outer diameter of the rolling piston under different operating conditions. It translates the volume of the wear incurred on the surface of the rolling piston to reduction of rolling piston outer diameter. Then the new value of the rolling piston radius is fed into the thermodynamic model to estimate volumetric and compression efficiencies of the compressor.

4.1 Wear Model

The roller and vane of rolling piston rotary type compressor are designed to be in loaded contact during normal operation. Relative motion between the vane tip and the roller when the compressor is running can lead to mild or sever wear of these two parts. The primary purpose of using oil as lubrication in the compressor is to reduce or ideally speaking, eliminate the wear which occurs at the roller/vane interface as well as other metal-to-metal contacts within the compressor. The long term reliability of the rotary compressor is proportional to the severity and amount of the wear which happens at these contact points.

Wear is the result of different mechanisms including fatigue, adhesion, abrasion and chemical corrosion [Sarkar, 1980]. Influence of each of these wear mechanisms depends on the regime of lubrication which exists at the roller/vane interface. Section 4.1.1 describes and analyzes the roller/vane contact lubrication regime and concludes that most likely boundary lubrication regime exists at the contact area.

4.1.1 State of Lubrication at Roller/Vane Contact

The regime of lubrication seen at the roller/vane contact depends on the operating conditions of the compressor. The possible regimes include hydrodynamic, elasto-hydrodynamic (EHD), partial EHD, and boundary-lubrication regimes [Jenkins, 1998].

In hydrodynamic lubrications, the sliding surfaces are completely separated by a relatively thick film of lubrication, and the normal force is supported by the pressure

within this film, which is generated hydrodynamically [Hutchings, 1992]. In this regime of lubrication the opposing surfaces must be conformal. Conformal surfaces means that the two opposing surfaces must be closely matched in dimensions and be separated by a small gap over a relative large area. As Figure 7 shows oil flows and creates a hydraulic pressure between the two surfaces. Under perfect conditions this type of lubrication will not allow wear. But in reality, this is not always the case.

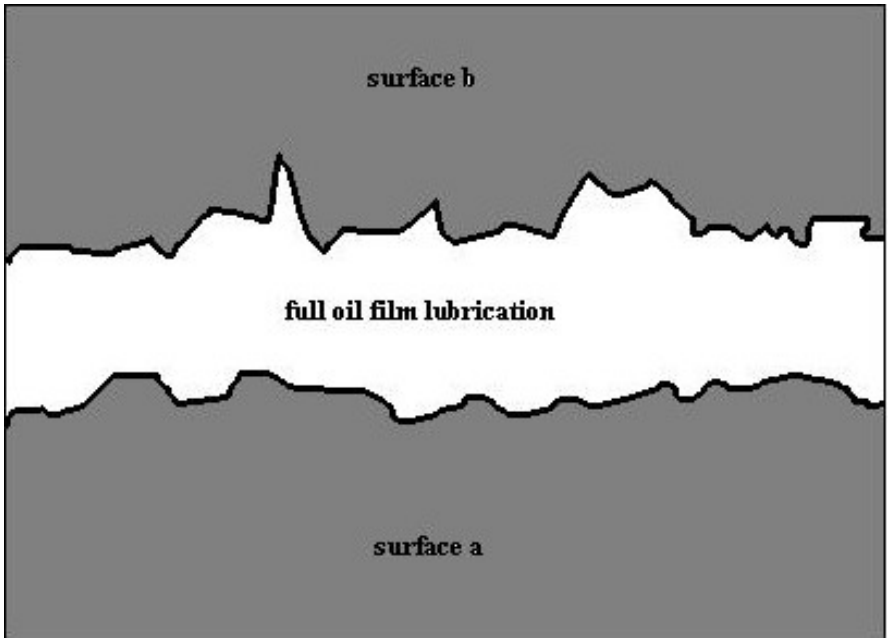

Figure 7: Hydrodynamic Lubrication Regime

If sliding surfaces are non-conformal and involve nominally line or point contact, then the local pressures in the contact zone will generally be much higher than those encountered in hydrodynamic lubrication. This particular state of the lubrication is called elasto-hydrodynamic (EHD).

The contact between gear teeth, between a cam and its follower, or at the vane and rolling piston contact area, all involve concentrated contacts of small area. Here the local pressure between the components is much higher compared to hydrodynamic lubrication. Under these conditions the dependence of the lubricant viscosity on pressure plays an important role as the elastic deformation of the bearing surfaces. [Hutchings, 1992]. The EHD film thickness is usually about three times the composite surface roughness of the sliding surfaces [Hamrock, 1989]. If the film thickness is smaller than the mentioned amount, then the state of the lubrication is partial-EHD. Usually, the asperities of the mating surfaces come into contact when lubrication state is partial-EHD.

When the contact load is very large, or the speed of the sliding surface is very low, it is almost impossible to maintain even a thin EHD film thickness and usually the surfaces asperities come into direct contact. In this case the sliding surfaces are protected by boundary lubrication [Hamrock, 1989]. Boundary lubrication regimes are formed by adsorbed molecular film on the surfaces. Repulsive forces between these films carry much of the load. So the direct contact between the asperities is avoided and as the result the amount of friction and wear will be reduced. Figure 5 shows a magnified image of two mating surfaces which the lubrication between the surfaces is in boundary lubrication regime.

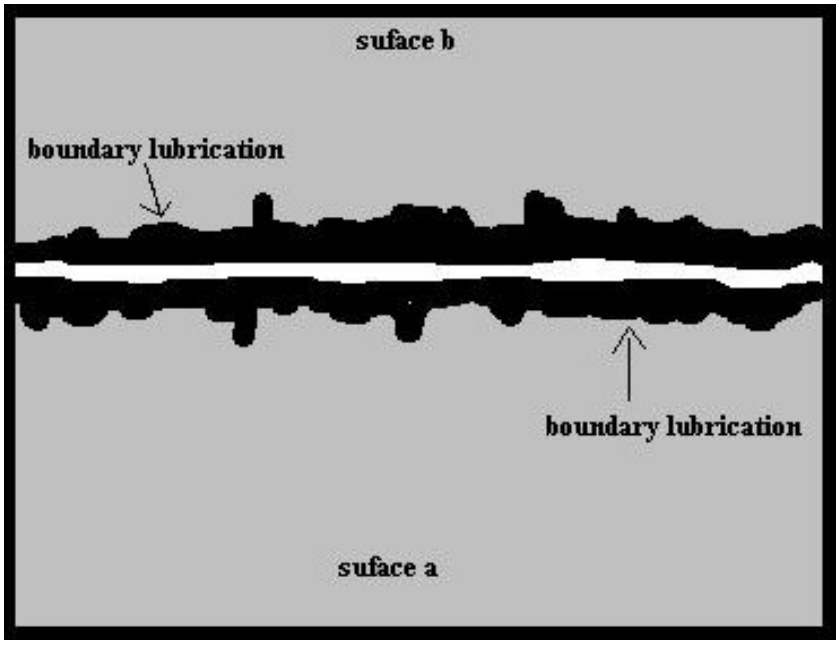

Figure 8: Boundary Lubrication Regime

In rolling piston rotary type compressors, adsorbed layers can be formed from lubricating oil molecules as well as the refrigerant molecules. The chlorine present in CFCs and HFCs refrigerants is known to form adsorbed layers. The absence of chlorine in HFC refrigerants can be one reason that at the piston/vane contact more wear is observed when these refrigerants are used [Hamrock, 1989].

Theoretically, there should be no wear at the piston/ vane contact point when the lubrication is in hydrodynamic or EHD regime, because there is no direct metal to metal contact. Hydrodynamic lubrication regime can not possibly exist because the geometry of piston/vane contact is non-conformal. EHD lubrication regime exist when the thickness of the oil film is large compared to the surface roughness of the piston/vane contact area. If the film thickness in not large enough to be in EHD regime, then partial-

EHD or boundary lubrication regimes will be resulted. Metal to metal contact occurs under the two later regimes and as the result wear can be observed.

Now we have to identify the lubrication regime at the piston/vane contact area. A complete analysis is presented in section 4.1.1.1 to check whether the lubrication oil regime is partial-EHD or boundary lubrication.

4.1.1.1 EHD Analysis of the Piston/Vane Contact

Elastohydrodynamic lubrication is a type of fluid-film lubrication in which the elastic deformation of the contacting surfaces is significant. The presence of EHD is generally found in high-loaded, non conformal, bearings and machine elements, like piston/vane interface in rolling piston rotary type compressors. The elastic deformation of the contacting surfaces results in a greater fluid-film thickness than what is predicted by the theory of rigid body hydrodynamic lubrication. Additionally, the high contact pressures with the region of contact can greatly increase the viscosity of the lubricant. These effects combine to enhance the load carrying ability of the lubricating fluid-film. In general, metal-to-metal contact will not occur if the minimum lubricant film thickness is at least three times the composite surface roughness of the contacting surfaces.

Analysis of EHD lubrication problems requires solving the coupled Reynolds, rheology, and elasticity equations [Hamrock, 1989]. Analytical solution is only possible for some special cases, since the Reynolds equation is a nonlinear differential equation. Based on the study that Pan and Hamrock [1989] has conducted, the numerical solution of the EHD

problem has led to a number of empirical correlations relating the operating condition, performance parameters, including minimum film thickness correlation given by:

$$\frac{h_{\min}}{R_{EQ}} = 1.174(W')^{-0.128} U^{0.694} G^{0.568}$$ Equation 5 [Hamrock 1989]

where the dimensionless load parameter W' is:

$$W' = \frac{F_N}{E' R_{EQ} L_p}$$ Equation 6 [Hamrock 1989]

the dimensionless speed parameter W' is

$$U = \frac{\mu_0 v_{rel}}{E' R_{EQ}}$$ Equation 7 [Hamrock 1989]

and the dimensionless material parameter G is:

$$G = \alpha E'$$ Equation 8 [Hamrock 1989]

The effective modulus of elasticity, E', and the equivalent radius, R_{EQ}, can be calculated with the following equations:

$$\frac{1}{E'} = \frac{1}{2}\left[\frac{1-v_v^{\,2}}{E_v} + \frac{1-v_p^{\,2}}{E_p}\right]$$ Equation 9 [Hamrock 1989]

Where v_v and v_p are the vane's and rolling piston Poisson's ratio, respectively.

$$\frac{1}{R_{EQ}} = \frac{1}{R_v} + \frac{1}{R_p}$$ Equation 10 [Hamrock 1989]

The lubricant film thickness $h_{\min}$ is calculated using Equation 5 for a rotary compressor under normal operating condition which is summarized in

Table 9.

Table 9: Standard Operating Condition

Test Condition	Standard
Discharge Pressure [kPa]	2,146
Suction Pressure [kPa]	626
Suction Superheat [°C]	11

Table 10 summarizes the EHD lubrication analysis.

Table 10: Rolling Piston/Vane Lubrication EHD Analysis at Normal Operation

Parameter	Value	Source
R_p	18.9895 mm	Samsung Correspondence
R_v	4.9 mm	Samsung Correspondence
R_{EQ}	3.89 mm	Samsung Correspondence
L_p	27.4895 mm	Samsung Correspondence
E_p	100 Gpa	Jenkins 1998
E_v	207 Gpa	Jenkins 1998

v_p	0.211	Jenkins 1998
v_v	0.295	Jenkins 1998
E'	143 Gpa	Hutchings 1992
α	15.0 $[Gpa]^{-1}$	Hutchings 1992
μ_0	8×10^{-3} Pa.s	Hutchings 1992
F_N	171 N	Modeling Results
v_{rel}	1.78 m/s	Modeling Results
W'	0.1118×10^{-4}	Equation 6
U	0.124×10^{-10}	Equation 7
G	2147	Equation 8
h_{min}	0.041 μm	Equation 5

Lubrication film at the rolling piston/vane interface is predicted to be 0.041 μm. The machined surface roughness of the piston and vane is 0.3 μm. The ratio of lubrication thickness to composite surface roughness indicates the regime of the lubrication [Hutchings 1992]. For this case, this ratio is 0.14 which falls in boundary lubrication regime.

4.1.2 Wear at the Piston\Vane Interface

Now that the lubrication regime at the piston\vane interface is known, the predominant wear mechanism at this lubrication regime needs to be identified. The term wear means surface damage or material removal from one or both solid surfaces in a sliding, rolling, or impact motion relative to one another [Bhushan, 1999]. In most cases wear occurs through surface interactions at asperities.

Adhesive wear is the predominant wear mechanism under boundary lubrication regime [Jenkins, 1998]. In adhesive wear, asperities on the two surfaces protrude through the lubricant film and interact. This interaction results in plastic yielding and subsequent material removal by sliding shear [Sarkar, 1980].

In order to model the adhesive wear which occurs at the piston/vane contact area, a simple theoretical analysis of adhesive wear which was originally introduced by Holm and Archard is used [Bhushan, 1999]. Archard showed that the volume of wear which occurs at the contact surface of two sliding surfaces is proportional to the applied normal load, F_N, and the sliding distance, S, and inversely proportional to the hardness of the surface which is worn away [Bhushan, 1999]. Archard wear equation can be written as follows [Bhushan, 1999]:

$$V_{wear} = K_{wear} \frac{F_N S}{H} \qquad \text{Equation 11}$$

constant K_{wear} is called wear coefficient which is a dimensionless number and it is always less than unity. This coefficient is of fundamental importance, and provides a valuable means of comparing the severity of wear processes in different systems. However, for engineering applications the quantity $\frac{K_{wear}}{H}$ is often more useful. This is usually given the symbol k which is called dimensional wear coefficient. k has a unit of $mm^3(Nm)^{-1}$, and represents the volume of material removed by wear in mm^3, per unit of sliding distance in meters, per unit of normal load at the contact area in N.

In this special case which a rolling piston rotary type compressor is being analyzed, Equation 11 can be expressed as:

$$\Delta V(i) = k \cdot F_N(i).|v_{rel}(i)|.\Delta t \qquad \text{Equation 12}$$

where $\Delta V(i)$ is the volume of the wear in mm^3 which occurs at each angle of rotation of the shaft

F_N is the normal force exerted on the piston/vane contact area

$v_{rel}(i)$ is the tangential relative velocity of the vane and rolling piston

Δt is the time step taken within the pump model

So the volume of the wear which occurs in one full rotation of the shaft can be expressed as:

$$V_{wear} = \sum_{\theta=0}^{2\Pi} \Delta V(i) \qquad \text{Equation 13}$$

As it was illustrated in Equation 12, F_N and $v_{rel}(i)$ needs to be calculated in order to be able to calculate the amount of wear. As the result, a complete force analysis should be done on the vane and roller which is presented in the following section.

4.1.3 Force analysis on the Piston and Vane

A complete dynamic analysis was performed on the vane and rolling piston to calculate F_N and $v_{rel}(i)$ which is presented in the following section.

4.1.3.1 Vane Dynamic

Many forces act on the compressor vane including pressure forces, spring force, lubricant oil shear force, and normal and tangential contact forces at the piston/vane interface. The contact forces, together with the relative velocity between the piston and vane, influence the amount of wear which occurs by the vane tip on the piston outer diameter.

The method used to calculate the vane forces are presented in the remainder of the section 4.1.3. The forces which act on the vane are shown in Figure 9.

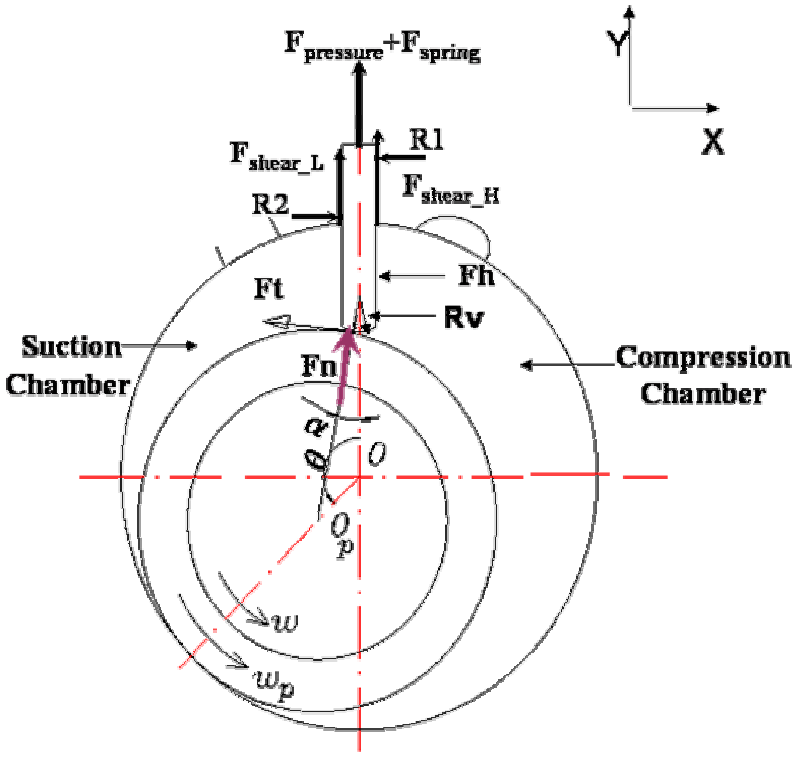

Figure 9: Force Analysis on the Vane

4.1.3.1.1 Vane Pressure Force

The tip of the vane is exposed to the suction pocket pressure, P_L, on one side and the discharge pocket pressure, P_H, on the other. The back of the vane is exposed to the constant discharge pressure, P_{dis}. These pressures and their corresponding surface areas combine and form the vane pressure force.

As the compressor shaft rotates, the point of contact between the piston and the vane tip changes. As the consequence, the area of the vane tip exposed to either the suction or discharge pocket changes as well. The projected area normal to the length of the vane is used to determine the normal pressure force acting on the vane. The projected area exposed to the suction pocket is expressed as:

$$A_L = L_P(\tfrac{1}{2}t_{vane} - R_v \sin\alpha)$$ Equation 14

and projected area exposed to the discharge pocket is:

$$A_H = L_P(\tfrac{1}{2}t_{vane} + R_v \sin\alpha)$$ Equation 15

where L_p is the height of the vane which is the same as height of the cylinder, t_{vane} is the thickness of the vane, R_v is the radius of the tip of the vane, and α is the piston\vane contact angle. The net force acting on the vane due to the mentioned pressures are:

$$F_{\mathrm{Pressure}} = P_L A_L + P_H A_H - P_{dis}(L_P \cdot t_{vane})$$ Equation 16

4.1.3.1.2 Vane Spring Force

The spring which is located at the back of the vane exerts force on the vane as well which depends on the displacement of the vane. From the compressor geometry, the displacement of the vane is:

$$y_{vane} = (R_p + R_v + e) - e\cos(\theta) - (R_p + R_v)\cos(\alpha)$$ Equation 17

where R_p the radius of the rolling piston and e is the shaft eccentricity.

Therefore the spring force is:

$$F_{spring} = k_{spring}(y_{vane} - y_0)$$ Equation 18

Where y_0 is the initial spring deflection at θ_s=360° and k_{spring} is the spring constant.

4.1.3.1.3 Vane Shear Force

In order to calculate the shear force acting on the vane due to the lubricating oil as the vane slides within the vane slot, the flow through the vane/vane-slot channel has to be analyzed. The flow through the vane/vane-slot channel is described is section 4.1.3.1.3.1 .

4.1.3.1.3.1 Flow through Vane/Vane-Slot Clearance

The flow of mixture of lubricant and refrigerant through the vane/vane slot clearance is modeled as flow between two parallel plates. The flow is assumed to be fully developed, steady, laminar, incompressible, and one dimensional. It is also assumed that the vane is parallel to and centered within the vane slot.

The infinite parallel-plate flow channel formed by the vane and vane-slot is shown in Figure 10. This figure shows the dimensions of the flow channel, the upstream and downstream pressures, and the velocity of the top and bottom plates. The length of the vane slot length is l_{slot}, the width is the height of the piston, L_p, and the height of is the vane/vane-slot clearance, δ_{vs}. The upstream pressure is the discharge pressure, P_{dis}, and the downstream pressure is the pocket pressure which is either P_L or P_H.

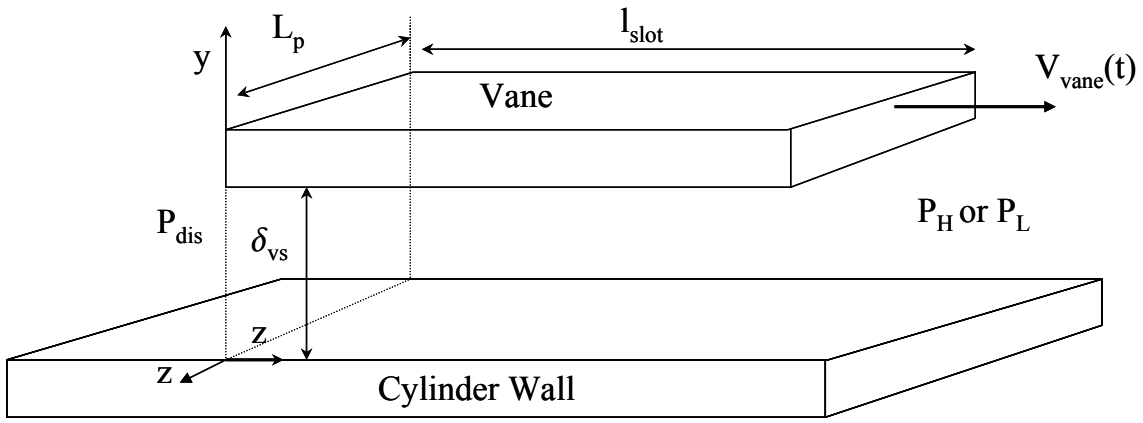

Figure 10: Vane/Vane-Slot Flow through Channel

Navier – Stokes equation was used to model the flow through the vane/vane-slot channel. Employing the aforementioned assumptions, the Navier-Stokes equations reduce to:

$$\frac{dp}{dx} = \mu_{oil} \frac{\partial^2 u}{\partial y^2}$$ Equation 19

where μ_{oil} is the viscosity of the refrigerant/oil mixture. Upon integration, the velocity profile is:

$$u(y) = \frac{1}{2\mu_{oil}} \frac{dp}{dx} y^2 + C_1 y + C_2$$ Equation 20

The boundary conditions on the velocity profile are:

$$u(0) = 0$$ Equation 21

$$u(\delta_{vs}) = V_{vane}$$ Equation 22

V_{vane} is the velocity of the vane which is a function of ω_s and θ. It can be derived by taking the first derivative of y_{vane} which is given by Equation 23.

$$V_{vane} = (R_p + R_v) \cdot \sin(\alpha) \cdot \frac{d\alpha}{dt} + e \cdot \omega_{shaft} \sin(\theta) \quad \text{Equation 23}$$

$$\frac{d\alpha}{dt} = \frac{e \cdot \omega_{shaft} \cdot \cos(\theta)}{(R_p + R_v) \cdot \cos(\alpha)} \quad \text{Equation 24}$$

Applying the boundary conditions to the problem, the velocity profile can be derived as shown in Equation 25:

$$u(y) = \frac{1}{2\mu_{oil}} \frac{dp}{dx}(y^2 - \delta_{vs} y) + \frac{V_{vane}}{\delta_{vs}} y \quad \text{Equation 25}$$

The pressure gradient $\frac{dp}{dx}$ is evaluated separately for each cylinder pocket. For the side of the vane open to the suction pocket, the pressure gradient is:

$$\frac{dp}{dx} = \frac{P_{dis} - P_L}{l_{slot}} \quad \text{Equation 26}$$

For the side of the vane open to the discharge pocket, the pressure gradient is:

$$\frac{dp}{dx} = \frac{P_{dis} - P_H}{l_{slot}} \quad \text{Equation 27}$$

Now that the velocity profile in the vane/vane-slot has been analyzed, the shear force acting on the vane can be calculated.

Shear stress can be calculated by the following equation:

$$\tau = -\mu_{oil} \frac{\partial u}{\partial y} \qquad \text{Equation 28}$$

where $\frac{\partial u}{\partial y}$ can be derived from Equation 25:

$$\frac{\partial u}{\partial y} = \frac{1}{2\mu_{oil}} \cdot \frac{dp}{dx} \cdot \delta_{vs} + \frac{V_{vane}}{\delta_{vs}} \qquad \text{Equation 29}$$

where the pressure gradients are presented by Equation 26 and Equation 27.

So the shear force can be expressed as:

$$F_{shear} = L_p \cdot l_p \cdot (\tau_L + \tau_H) \qquad \text{Equation 30}$$

where τ_L is the shear stress on the suction side of the vane and τ_H is the shear stress on the discharge side of the vane.

4.1.3.1.4 Piston/Vane Contact Force

The vane forces mentioned above, together with the vane inertia, combine and produce the normal and tangential (friction) contact force between the piston and vane. The magnitude of the normal force is found by summing the vane forces in the y-direction.

$$\sum F_y = m_{vane} a_{vane} = F_N \cos\alpha + \mu_{friction} F_N \sin\alpha + F_{pressure} + F_{spring} + F_{shear} \qquad \text{Equation 31}$$

where m_{vane} is the mass of the vane, a_{vane} is the acceleration of the vane which can be derived but taking the derivative of Equation 23, $\mu_{friction}$ is the coefficient of friction between the vane and piston, and α is the contact angle.

Equation 32:

$$a_{vane} = (R_v + R_p)\cdot\cos(\alpha)\cdot(\frac{d\alpha}{dt})^2 + e\cdot\omega_s\cdot\sin(\alpha)\cdot(\frac{-\omega_s\cdot\sin(\theta)\cdot\cos(\alpha)+\frac{d\alpha}{dt}\cdot\sin(\alpha)\cdot\cos(\theta)}{(\cos(\alpha))^2}) + e\cdot\omega^2\cdot\cos(\theta)$$

So the normal force F_N can be expressed as:

$$F_N = \frac{m_{vane}a_{vane} - F_{pressure} - F_{spring} - F_{shear}}{\cos\alpha + \mu_{friction}\sin\alpha} \qquad \text{Equation 33}$$

4.1.3.2 Sliding Velocity at Vane Tip and the Rolling Piston

Relative velocity at the vane tip and the rolling piston surface can be obtained by solving Equation 34 [Sakania et. al. 1984].

$$v_{rel} = R_p\cdot\omega_p + e\cdot\omega_s\cdot\frac{\cos(\theta)}{\cos(\alpha)} \qquad \text{Equation 34}$$

As it is shown in the above equation, ω_p which is the angular velocity of the rolling piston has to be known. As the shaft rotates different torques which act upon the rolling piston during the compression cycle change as well and the consequence the angular velocity of piston change continuously. Changes in relative velocity due to changes in ω_p directly affect the amount of wear incurred by the piston and the vane tip. The

relationship between the resultant torques acting upon an object with its angular velocity is shown in Equation 35:

$$\sum T = I \cdot \dot{\omega}_p \qquad \text{Equation 35}$$

In order to calculate ω_p a full dynamic analysis has to be done on the rolling piston.

4.1.3.3 Rolling Piston Dynamics

Four different torques act upon the rolling piston throughout the compression cycle which are torque acting on the piston due to piston/vane contact, torque due to piston/shaft shear force, torque due to piston/cylinder shear force and finally torque due to piston/bearing shear force.

Modeling of the aforementioned torques is presented in the remainder of this section.

4.1.3.3.1 Piston Torque due to Piston/Vane Contact

The friction force which acts at the contact area of the vane and rolling piston produces a torque about the piston center of rotation. The magnitude of this torque is:

$$T_p^{pv} = \pm \mu_{friction} \cdot F_N \cdot R_p \qquad \text{Equation 36}$$

where F_N is expressed by Equation 33

The relative tangential velocity between the piston and vane determines the direction of this torque. Specifically, torque always opposes relative velocity.

4.1.3.3.2 Piston Torque due to Piston/Shaft Clearance

The shear force which act due to the lubricating oil between the piston inner diameter and the shaft eccentric outer diameter results in a torque which act on the piston. Assuming the piston is centered on the shaft eccentric such that the radial clearance is constant around the piston, the shear stress can be determined by modeling the clearance as a parallel plate flow channel. Assuming the oil behaves as a Newtonian fluid, the shear stress on the piston inner diameter is:

$$\tau = \mu_{oil} \frac{\omega_p R_{inner}}{\delta_{ps}} \qquad \text{Equation 37}$$

where R_{inner} is the inner radius of the piston and δ_{ps} is the clearance between the shaft eccentric and piston diameter. The shear force acting on the piston inner diameter is therefore:

$$F = \tau \cdot A = \mu_{oil} \frac{\omega_p R_{inner}}{\delta_{ps}} (2\Pi \cdot R_{inner} \cdot l_{ps}) \qquad \text{Equation 38}$$

The resulting torque on the piston is:

$$T_p^{ps} = F \cdot R_{inner} = 2\Pi \mu_{oil} \omega_p \frac{{R_{inner}}^3 l_{ps}}{\delta_{ps}} \qquad \text{Equation 39}$$

4.1.3.3.3 Piston Torque due to Piston/Cylinder Wall Clearance

The flow of oil and refrigerant mixture through the piston/cylinder wall clearance produces a torque on the piston. With Newtonian fluid assumption, the shear force due to the oil flow is:

$$F = \mu_{oil} L_p l \frac{\partial u}{\partial y} \qquad \text{Equation 40}$$

where l is the length of the flank leak path. Preissner (2001) showed that the length of the flank leak path can be expressed as the curvature difference *cd*

cd= 1/r – 1/R

where r and R are the radii of the channel wall with the smaller and greater curvature, respectively. In the piston and cylinder wall case r is the radius of the piston, R_p, and R is the radius of the cylinder, $R_{cylinder}$. $\frac{\partial u}{\partial y}$ can be calculated by analyzing the mixture flow through the piston/cylinder wall.

The velocity of the cylinder wall is zero and the velocity of the rolling piston surface results from the shaft and rolling piston rotation:

$$u_p(t) = \omega_s (R_p + e) - \omega_p R_P \qquad \text{Equation 41}$$

The flow velocity profile across the clearance between the rolling piston and cylinder wall is:

$$u(y,t) = \frac{1}{2\mu_{oil}} \frac{dp}{dx} (y^2 - \delta_{pw} y) + \frac{u_p}{\delta_{pw}} y \qquad \text{Equation 42}$$

where the pressure gradient is:

$$\frac{dp}{dx} = \frac{P_H - P_L}{l} \qquad \text{Equation 43}$$

The torque on the rolling piston due to the shear stress acting on the piston is:

$$T_p^{pw} = \mu_{oil} \cdot L_p \cdot l \cdot R_{piston} \cdot \frac{\partial u}{\partial y} \qquad \text{Equation 44}$$

4.1.3.3.4 Piston Torque due to Piston/Bearing Plate Clearance

The mixture of oil and refrigerant which flows through the piston/bearing plate clearance is somehow complex. When modeling the flow through this clearance only the pressure driven (radial) flow was considered. This radial flow does not produce a torque about the center of the piston. However, the torque produced can be approximated by considering only the flow induced by the piston and shaft motion.

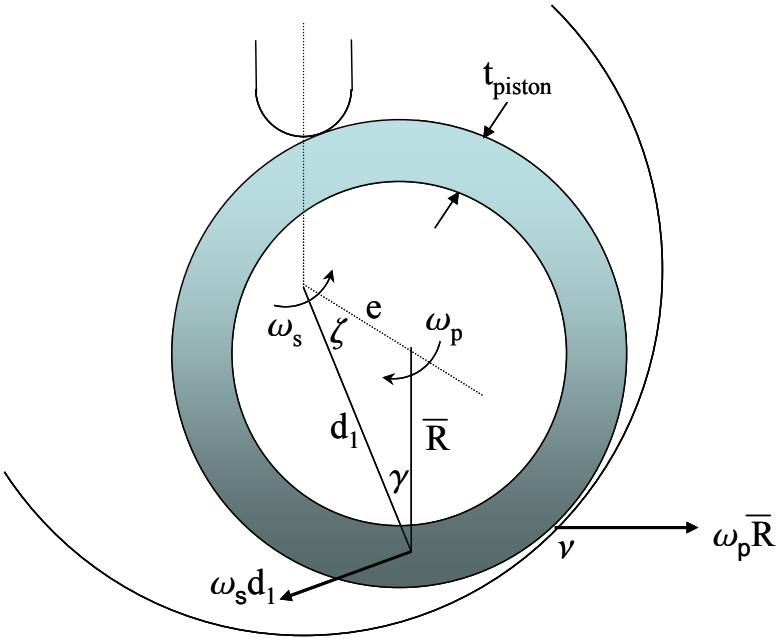

Figure 11: Piston/Bearing Plate Clearance Torque

As it is shown in Figure 11, the tangential (i.e. normal to the piston radius) piston velocity at the midpoint of the piston thickness is given by:

$$\nu = \omega_p \bar{R} - \omega_s d_1 \cos\gamma \qquad \text{Equation 45}$$

where $\bar{R}$ is the average of the piston inner and outer radii, and the distance d_1 and the angle γ are:

$$\gamma = \sin^{-1}[\frac{e}{R}\sin\xi] \qquad \text{Equation 46}$$

$$d_1 = e\cos\xi + \bar{R}\cos\gamma \qquad \text{Equation 47}$$

The flow velocity profile is assumed to be linear with the maximum value at the piston surface and zero value at the bearing surface. The shear stress is then given by:

$$\tau = \mu_{oil} \frac{v}{\delta_{pb}}$$ Equation 48

The shear force acting on the piston at a particular angle, $d\xi$, is:

$$dF = \mu_{oil} \frac{v}{\delta_{pb}} t_{piston} d_1 d\xi$$ Equation 49

And the incremental torque is:

$$dT = \frac{\mu_{oil} \cdot t_{piston}}{\delta_{pb}} [\omega_p d_1 \bar{R}^2 - \omega_s d_1^2 \bar{R} \cos\gamma] d\xi$$ Equation 50

The net torque acting on the piston due to the flow through the piston/bearing clearance is found by integrating Equation 50 over the top and bottom surfaces of the piston which means ξ varies from 0 to 2π :

$$T_p^{pb} = -2 \frac{\mu_{oil} \cdot t_{piston}}{\delta_{pb}} [\omega_p I_1 - \omega_s I_2]$$ Equation 51

Where factor 2 takes into account the top and bottom surfaces of the piston. The values of I_1 and I_2 can be calculated with the following equations:

$$I_1 = \int_0^{2\Pi} \bar{R}^2 (e\cos\xi - \bar{R}\cos\gamma) d\xi$$ Equation 52

$$I_1 = \int_0^{2\Pi} \bar{R} (e\cos\xi - \bar{R}\cos\gamma)^2 \cos\gamma d\xi$$ Equation 53

4.1.3.3.5 Piston Angular Velocity

The torques which act on the piston cause the rotational speed of the piston which rotates about the shaft eccentric to vary during the compressor cycle. The piston angular acceleration, $\dot{\omega}_p$, is calculated using Equation 35. I in the mentioned equation is the rolling piston inertia which can be found by using the equation below:

$$I_p = \tfrac{1}{2}\Pi\rho_p L_p (R_p{}^4 - R_{inner}{}^4) \qquad \text{Equation 54}$$

The change in the piston angular velocity is then found by taking a forward Euler step:

$$\omega_p^{i+1} = \omega_p^i + \dot{\omega}_p \cdot \Delta t \qquad \text{Equation 55}$$

where Δt is the time step taken into the simulation program. So ω_p can be calculated at each angle of rotation of the shaft.

The whole purpose of calculating ω_p was to be able to calculate v_{rel}. In order to solve for v_{rel} equations 34 through 55 has to be solved. The mentioned equations result in a set of coupled equations which a non linear equation solver was used to solve them. To serve this purpose, this set of equations was solved in EES (Engineering Equation Solver).

4.2 Thermodynamic Model

The thermodynamic process is formulated using conservation of mass and energy, resulting in a system of ordinary differential equations (ODE) with two variables. Systems of ODE's are traditionally solved by dividing the process into discrete time steps

of variable size. The algorithm that has been developed calculates the performance of the devices accounting for valve losses, internal leakage, and internal heat transfer [Huff, 2003]

Inputs to the program are the boundary conditions within which the compression takes place including geometric data of the rolling piston rotary type device. Output of the simulation is the thermodynamic state during the process, mass flow rate, work, and heat transfer to and from the fluid, and the gas forces and moments acting on the moving surfaces and the drive shaft. The algorithm is implemented in Matlab Release 12 and uses CEEEProps, which is an interface to Refprop 7, to calculate fluid properties. Refprop 7 is a library of refrigerant properties developed by the National Institute of Standards and Technology. CEEEProps provides wrapper libraries to Refprop 7 to accommodate access to the Refprop 7 property routines from Matlab. The simulation tool provides an interface to Microsoft Excel for batch operation [Huff, 2003].

The mechanism of rolling piston rotary compressors was explained in 2.4. The following section shows the importance of geometric data.

Geometric Data

The rotary piston mechanism can be approximated by a small circle orbiting around the center of a larger circle with an eccentricity equal to the difference between the diameters of the circles. The base area of the chamber volume at rotation angle α can be approximated by difference between the areas of the section around the cylinder center, labeled A_1 in Figure 12 and limited by points P_S and P_C, the section around the piston center, A_2 in Figure 12 is limited by points P_V and P_C, and the triangle between the contact point of piston and vane, P_V, and the circle centers labeled A_3. The volume is obtained by multiplying the resulting base area with the cylinder height.

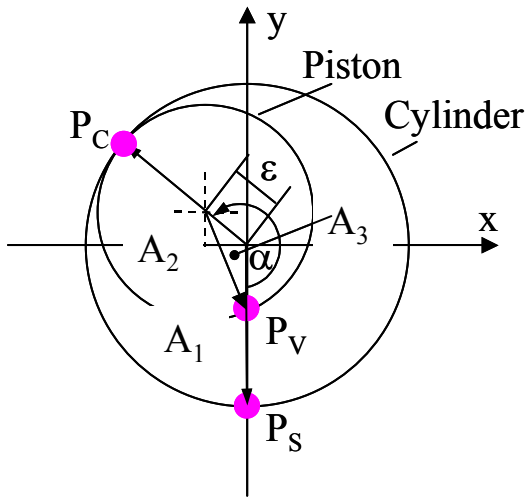

Figure 12: Schematic of Rotary Piston Mechanism [Huff, 2003]

The points P_V and P_C can be found from the description of a circle orbiting around the center of a larger circle. The eccentricity of the inner circle, ε in Figure 12, is given by the difference between the diameters of the circles. The contact point between the circles, P_C, is given be the orbiting angle, α, and the diameter of the larger circle. The contact

point between inner circle and vane, P_V, is given by the location of the intersection between negative y-axis and inner circle.

The rotary piston mechanism has five different leak paths, indicated by the solid arrows in Figure 3. The leaks across the piston wall, through the vane slot, and across the vane occur on the top and bottom of the device. These three leaks are tip leaks; the other two are flank leaks. In the thermodynamic model the dimensions of the flank leaks are constant and equal to the cylinder height during the entire process. In all other leaks, the width changes during the cycle. The width of the leak across the vane indicated by the line w_c in Figure 13, is equal to the distance between point where the vane penetrates the cylinder wall and the nose of the vane. The width of the leak across the piston wall, indicated by w_d and w_e in Figure 13, are given by the contact point of the vane on the piston and the contact point of piston and cylinder wall

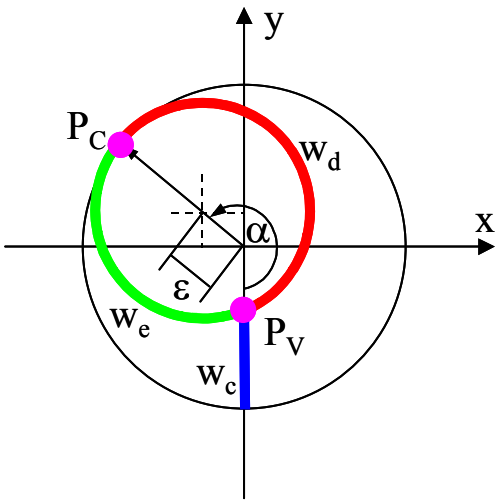

Figure 13: Width of variable leaks in rotary piston compressor

The pressure reservoirs communicating via the vane leak are the two pockets in the device. The pressures in both chambers vary during the entire process. Across the piston leaks communicate with the shell pressure. Hence, the pressure reservoirs associated with these leaks are constant during the entire process.

4.2.1 Modeling Approach

The algorithm is based on a discretization of the process into a number of time steps, following a control volume through the transient process from inlet, compression, or expansion to discharge. At each time step, the irreversible processes of mass and heat flow are estimated. During each time step, a number of parallel control volumes can exist simultaneously

4.2.1.1 Assumptions

Fluid Properties

The fluid properties in a control volume are average (bulk) properties. It is assumed that the properties are constant during each time step. The properties are calculated for thermodynamic equilibrium. Hence, the process is simulated as quasi-steady-state process.

Valves

Valves are modeled as ideal valves. In rolling piston rotary type compressor, the discharge valve is a pressure actuated valve and the suction valve in a position valve. In

the model pressure actuated valve (reed) is assumed to open fully and without any time delay. The position valve is assumed to open and close fully.

4.2.1.2 Geometric Data

Geometric information about the device is required at each time step. These data are:

- Rotation angle of crankshaft
- Control Volume
- Projection of moving surfaces into x-, y-, and z- direction
- Leak paths: The data for the leak path contain topological information about the device, indicating the pockets adjacent to the control volume being followed
- Dimensions of each leak path

The geometric information is provided in an ASCII text file.

4.2.1.3 Thermodynamic Simulation

Each time step is considered a sequence of two separate processes:

(1) Isentropic change of volume at constant change of volume at constant mass (process 1-2*)

$$s^*_2 = s_1 \qquad \text{Equation 56}$$

$$m^*_2 = m_1 \qquad \text{Equation 57}$$

$$\rho^*_2 = m^*_2 / V2 \qquad \text{Equation 58}$$

$$u^*_2 = u(s^*_2, \rho^*_2)$$ Equation 59

(2) Change of mass and internal energy due to mass and heat transfer at constant volume (process 2^*-2)

$$m_2 = m^*_2 + \sum m_{Valve} + \sum m_{Leak}$$ Equation 60

$$U_2 = u_2^* \cdot m_2^* + \sum H_{valve} + \sum H_{Leak} + \sum Q$$ Equation 61

$$u_2 = U_2 / m_2$$ Equation 62

$$\rho_2 = m_2 / V_2$$ Equation 63

$$s_2 = s(u_2, \rho_2)$$ Equation 64

4.2.1.4 Valve Flow

The instantaneous mass flow rates through the valves are simulated as incompressible flow through orifice.

(a) Single phase [White 1994]

$$\dot{m}_{Valve}(t) = C_d \cdot A_{Valve} \cdot \sqrt{\frac{2\rho_{up}\Delta P}{1-\beta^4}}$$ Equation 65

$$C_d(t) = 0.5959 + 0.0312\beta^{2.1} - 0.184\beta^8 + \left(0.0029\beta^{2.5}\right)\left(10^6 / Re(t)\right)$$ Equation 66

$$10^4 < Re < 10^7$$

$$\beta = 0.3$$ Equation 67

(b) Twp phase flow [Lin 1982]

$$\dot{m}_{Valve}(t) = C_d(t) \cdot A_{Valve}(t) \cdot \sqrt{\frac{2\rho_{up}(t)\Delta P(t)}{(1-\beta^4) \div \left[(1-x_{up})\Theta(t) + x_{up}\sqrt{\rho_L(t)/\rho_G(t)}\right]}} \quad \text{Equation 68}$$

$$\Theta(t) = 1.48625 - 9.26541 r_d(t) + 44.6954[r_d(t)]^2 - 60.615[r_d(t)]^3 - 5.12966[r_d(t)]^4 - 26.5743[r_d(t)]^5 \quad \text{Equation 69}$$

$$0.1 \le x \le 1.0, r_d \le 0.328, P/P_{crit} \le 0.8319$$

C_d and β are the same as for single phase flow.

The enthalpy flow rate through a valve is obtained by multiplying the mass flow rate with the upstream specific enthalpy. The valve flow is checked for choked flow by comparing the computed flow velocity against the speed of sound at the upstream conditions.

The effective flow area A_{Valve} is the cross sectional area of the port. Valve motion is not considered which result in overestimating the valve performance.

4.2.1.5 Heat Flow

The heat transfer in compressors has been studied by a number of researchers with contradicting results [Huff, 2003]. The instantaneous heat flow rate is described by Newton's approach.

$$\dot{Q}(t) = h(t) \cdot A_Q(t) \cdot [T_{Wall} - T(t)] \quad \text{Equation 70}$$

The heat transfer coefficient h(t) is obtained by the following equation:

$$h(t) = a[\mathrm{Re}(t)]^b . \mathrm{Pr}^c \quad \text{Equation 71}$$

The temperature T_{wall} is the effective wall temperature of the control volume. In a realistic compressor, the wall temperature varies with location and time. In the simulation however, an average time-independent wall temperature is assumed.

4.2.1.6 Leak Flow

Although internal leakage has significant effect on the performance of any type of positive displacement compressors, little research has been conducted to derive correlations of the instantaneous leakage mass flow rate dependent on geometry and driving pressure differences.

The instantaneous leak flow rates are computed assuming incompressible viscous flow and accounting for frictional losses and minor losses due to entrance and exit effects. The computed flow velocity is checked against the speed of sound and corrected for chocked flow rate as is computed as:

$$\dot{m}_{Leak}(t) = \sqrt[20]{[\dot{m}_{Leak}^{La\min ar}(t)]^{20} + [\dot{m}_{Leak}^{Turbulent}(t)]^{20}} \qquad \text{Equation 72}$$

$$\dot{m}_{Leak}^{La\min ar}(t) = \frac{-4\mu wL}{k_m} + \sqrt{(\frac{-4\mu wL}{k_m \delta})^2 + \frac{\rho(w\delta)^2}{k_m}\Delta P} \qquad \text{Equation 73}$$

$$\dot{m}_{Leak}^{Turbulent}(t) = \sqrt{\frac{\rho(w\delta)^2}{0.01875 \times L/\delta + k_m}\Delta P} \qquad \text{Equation 74}$$

The effective diameter is 2/3 of the hydraulic diameter (White, 1994), the friction factor for turbulent flow is 0.075 (fully rough flow channel), and the coefficient for minor losses is 1.5, assuming a coefficient of 0.5 for the entrance losses and 1 for the exit losses.

In rolling piston rotary compressors oil is used for sealing and also for lubrication of moving parts. When the compressor operates, oil and refrigerant mix together depending on the operating conditions. In this case, refrigerant leak from the discharge pocket to the suction pocket via a so-called oil-leak. Refrigerant dissolves in oil in the discharge pocket and evaporates from the oil as the mixture enters the suction pocket. In this case solubility and density of Mineral oil and R-22 is calculated based on the operating condition and then the kinematics viscosity of the mixture is calculated. When solubility is known, the amount of R-22 which evaporates when the oil-refrigerant mixture leaks to the suction pocket can be calculated.

4.2.1.7 Operating Parameters

The compressor and expander operate under a set of given operating parameters. These parameters are:

- Inlet pressure
- Inlet density
- Outlet pressure
- Wall temperature
- Angular speed

4.2.1.8 Solution Scheme

The simulation of the compression process consists of two problems:

a) Numerical integration of the transient process from suction to discharge

b) Numerical solution of the leakage flow rates to satisfy conservation of mass and energy.

The numerical integration solves the problem

$$f(t) = f_0 + \int y(f,t)dt \qquad \text{Equation 75}$$

where $f(t)$ is the mass or energy contained in the control volume, f_0 is an initial condition, $y(f, t)$ is the mass or energy flow rate and t is time. For the valve and heat flow rates, a fourth order Runge-Kutta method is used.

Using a step-by-step method such as Runge-Kutta for the leak flow rates may result in violation of conservation of mass or energy. The difference between valve and heat flow on the one hand and leak flow on the other hand is that valve and heat flow only affect the control volume on hand, while leak flow affects also control volumes of previous or future time steps. This is especially apparent in devices with several pockets interacting with each other, for example in a scroll compressor. Shortly after a control volume has been formed in the suction process, it may be connected via a leak with a pocket closer to the center of the scroll and some amount of mass may leak into the control volume, resulting in a pressure increase. After one rotation of the crankshaft, the control volume may be exactly at the point where the high-pressure pocket was. The control volume communicates now with a pocket closer to the perimeter of the scroll, which however,

has a higher pressure than at the previous instance. Thus, the pressure difference and hence the mass flow rate is smaller. Consequently, the control volume and the low-pressure pocket contain more mass than before, resulting in a violation of the conservation of mass (and energy as well as in the destruction of entropy, as can be shown).

In order to avoid this type of problem, the leak flow rates must be computed simultaneously for all time steps. To reduce the computational time for this procedure, the leak flow rates are computed with an explicit Euler scheme. Starting with an initial guess for the leak flow rates at all time steps (for instance all flow rates are zero), the integration is carried out, producing a mass and internal energy profile in the device for the time interval from suction to discharge. Based on this pressure profile, the leak flow rates are newly computed. In order for the solution to represent the compressor/expander at steady operation, the pressure and enthalpy field must not change when the newly computed leak flow rates are applied a second time. Conversely, the leak flow rates of two subsequent iterations must be equal. This means the leak flow rates must produce the same pressure and enthalpy field, which they were computed from

$$\dot{m}_{Leak} = F\left(\dot{m}_{Leak}\right)$$
$$\dot{H}_{Leak} = F\left(\dot{H}_{Leak}\right) \qquad \text{Equation 76}$$

where F is a system of equations describing the mass and energy field in the compressor/expander as variables. This can be interpreted as the flow rates being the eigenvector to the linear map F. This means that the solution flow rates are fixed points

to the system of equations *F*. Following these observations, Equation 76 is solved using a fixed-point iteration scheme

$$\dot{m}_{j+1}^{Leak} = F\left(\dot{m}_{j}^{Leak}\right)$$
$$\dot{H}_{j+1}^{Leak} = F\left(\dot{H}_{j}^{Leak}\right) \qquad \text{Equation 77}$$

Convergence is reached when

$$\left|\dot{m}_{j}^{Leak} - \dot{m}_{j-1}^{Leak}\right| < \varepsilon \text{ , or}$$
$$\left|\overline{P}_{j} - \overline{P}_{j-1}\right| < \varepsilon \qquad \text{Equation 78}$$

where $\overline{P}$ indicates the pressure field. The value for the convergence criterion should be established by solving the problem with increasing accuracy and observing when the change of the results levels off to an order of magnitude sufficient for the specific application.

4.2.1.9 Step Size Adoption

The error in the numerical integration depends strongly on the size of the time intervals. In order to reduce error while keeping the computational time within limits, the step size is refined only where the error is large. Two criteria are used to determine whether the step size has to be refined. The step size is reduced if the dependency of mass and internal energy on valve flow and heat transfer is strong

$$\left|\partial f_{j} / \partial y_{j}\right| \Delta t_{n} > \varepsilon_{1} \qquad \text{Equation 79}$$

where the criterion ε can be determined by the user. The second criterion is used for the leakage flow rates. The step size is reduced if the ratio of leak flow to mass contained in the pocket exceeds a user-defined limit:

$$\max\left(\left|m_J^{Leak} \middle/ m_j\right|\right) > \varepsilon_2 \qquad \text{Equation 80}$$

4.2.1.10 Performance Characteristics

The indicated and volumetric efficiencies are used to characterize the performance of the compressors analyzed. With a known displacement volume and the boundary conditions (inlet state, discharge pressure and possibly wall temperature) these parameters can be translated into the mass flow rate delivered and the work input or output. The indicated efficiency is defined as

$$\eta_{ind} = \left\{ \frac{W_{is}}{W_{ind}} = \frac{h(s_{in}, P_{out}) - h(s_{in}, P_{in})}{h(s_{out}, P_{out}) - h(s_{in}, P_{in})} \right. \qquad \text{Equation 81}$$

The volumetric efficiency η_{vol} is defined as

$$\eta_{vol} = \frac{\dot{m}_{real}}{\rho_{in} \cdot V_{displ}} \qquad \text{Equation 82}$$

where V_{displ} is the compressor displacement volume

5 Results and Discussion

5.1 Experimental Results

Four different test conditions were established in a technical discussion with the compressor manufacturer which is summarized in Table 11.

Table 11: Test Conditions

	Test A	Test B	Test C	Test D
Discharge Pressure [psi (Mpa)]	580 (4.00)	490 (3.38)	400 (2.76)	310 (2.14)
Suction Pressure [psi [MPa])	120 (0.83)	110 (0.76)	100 (0.69)	90 (0.62)
Pressure Difference [psi [MPa])	460 (3.17)	380 (2.62)	300 (2.07)	220 (1.52)
Condensing Temp. [°F (°C)]	184 (84.5)	169 (75.9)	151 (66.0)	130 (54.3)
Evaporating Temp. [°F (°C)]	62(16.7)	57 (13.7)	51 (10.4)	44 (6.9)

Test condition A, is very severe and based on previous experience it causes severe damage to the compressor components. The compressor was tested at condition B for 30 days. Figure 14 & Figure 15 show the performance and volumetric efficiency degradation over time. Volumetric efficiency dropped 4.35% over the period of test and also compressor's capacity degraded for about 2.53%.

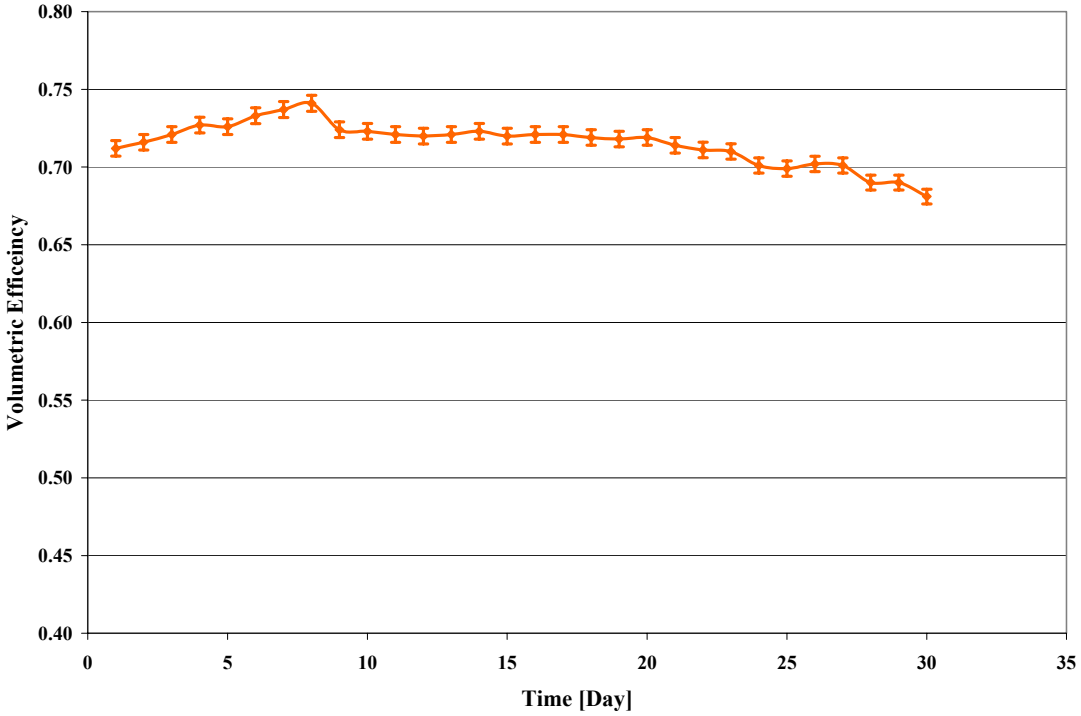

Figure 14: Degradation of Volumetric Efficiency over Time under Test Condition B

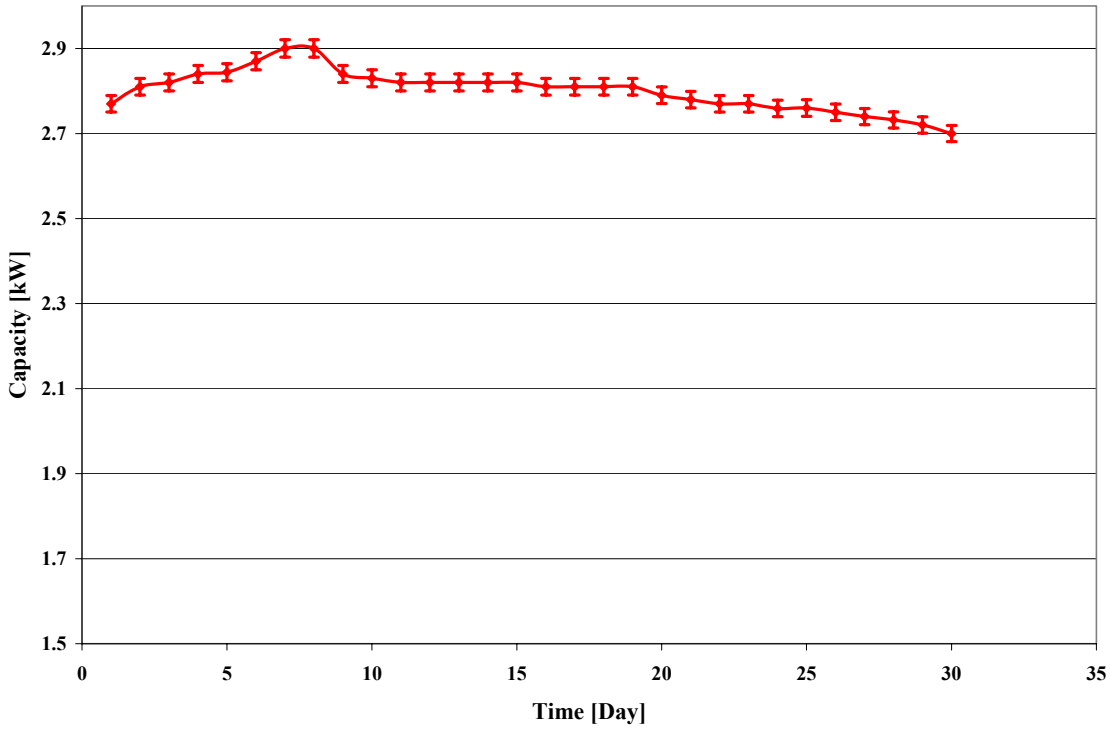

Figure 15: Degradation of Capacity over Time under Test Condition B

As it can be observed from Figure 14 & Figure 15 there is an initial increase in capacity and volumetric efficiency. This phenomenon can be explained by ageing effect of the material used in manufacturing of the compressors. The surface roughness and asperities of the two rubbing surfaces reduces at the beginning of compressor usage and it result in capacity and volumetric increase. After the initial increase in capacity and volumetric efficiency as the compressor runs longer its performance degrades due to increase in the amount of refrigerant leakage from suction pocket to discharge pocket.

5.2 Modeling Results and Verification of the Model

As it is shown in Figure 16, the normal contact force between the rolling piston and vane, given by Equation 33, varies over the compressor cycle. As the gas pressure in the discharge pocket increases [refer to Figure 17] the normal force between the rolling piston and vane decreases due to the fact that the vane is being pushed away from the roller. At shaft angle 2π when gas in the suction pocket has just sealed off and is transferred to discharge pocket, pressure is equal to the suction pressure.

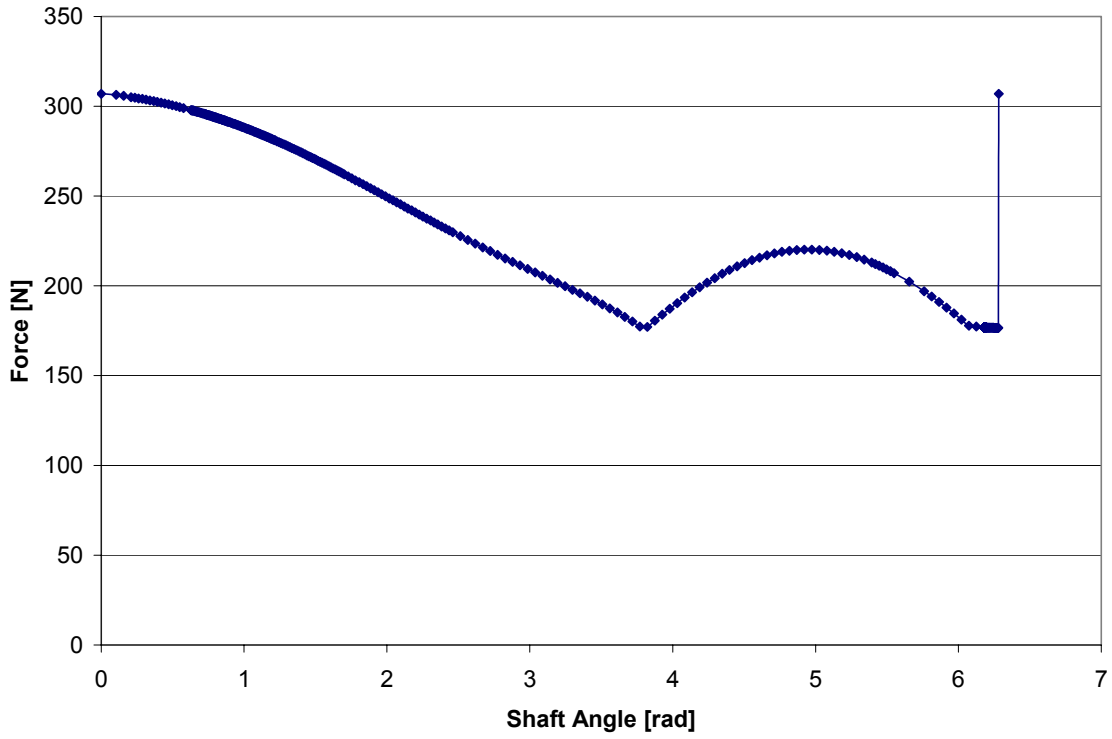

Figure 16: Rolling Piston/Vane Contact Force versus Shaft Angle

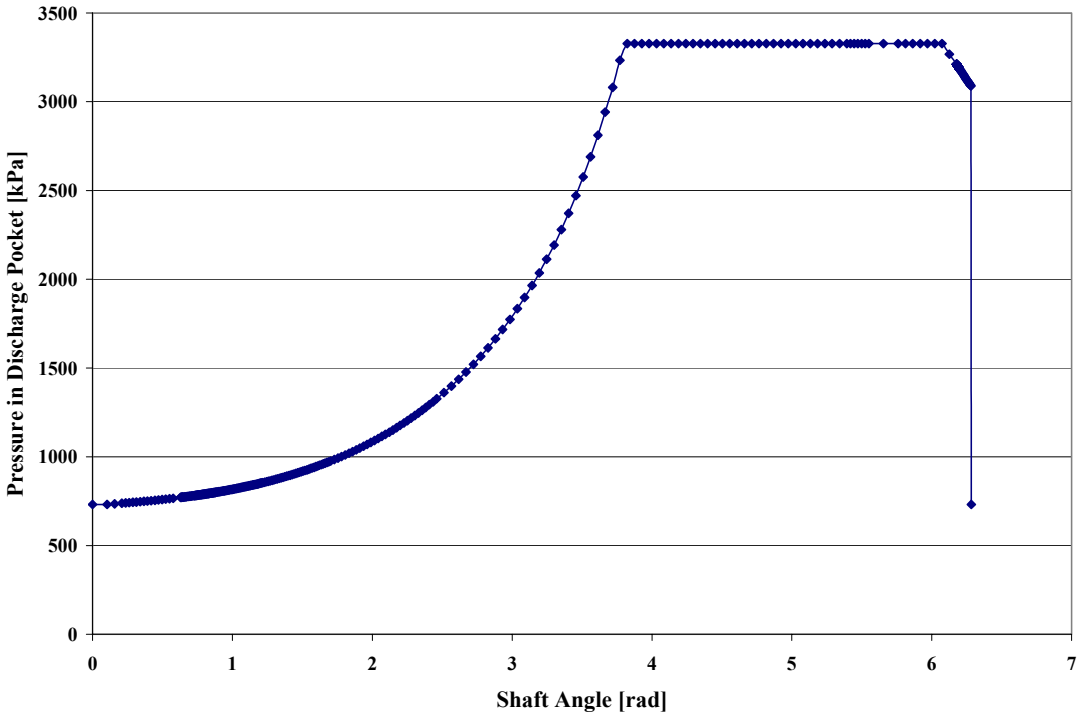

Figure 17: Gas Pressure in the Discharge Pocket

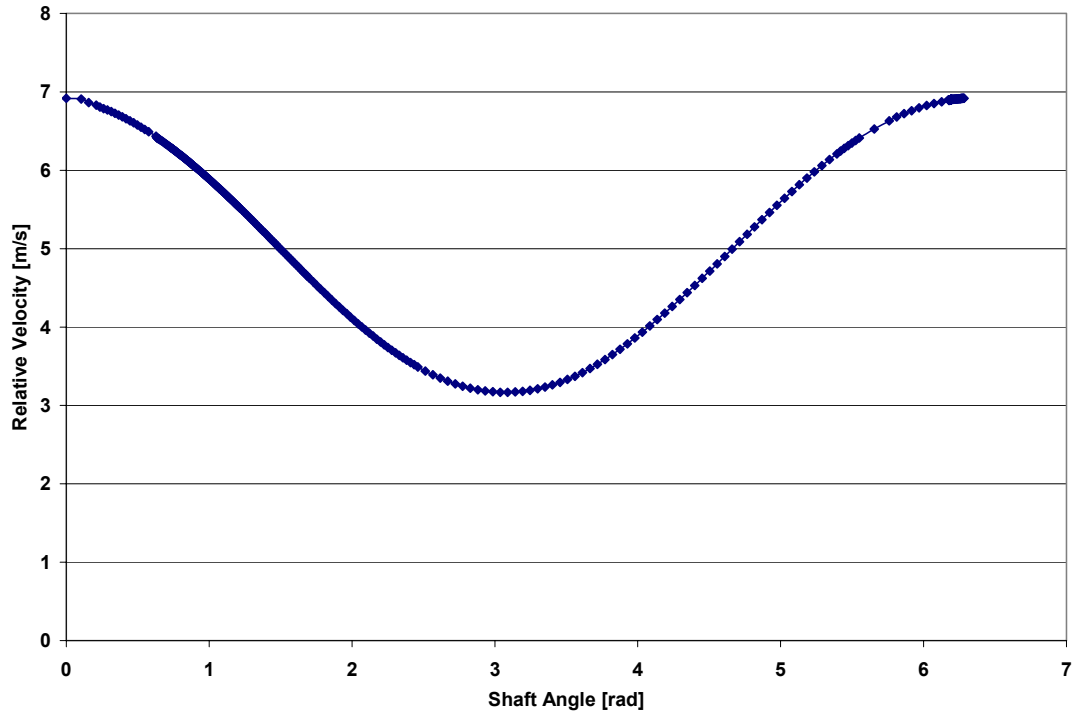

Figure 18: Rolling Piston/Vane Relative Velocity versus Shaft Angle

As shown in Figure 18, tangential relative motion between the rolling piston and the vane, given by Equation 34, has a symmetric pattern. The minimum velocity occurs at shaft angle π.

As it was explained in section 3.3 the outer diameter of the roller was measured before and after testing. The difference between the measured value before and after testing was 3 μm. This means that wear on has resulted in 3 μm reduction in outer diameter of the rolling piston. This value is predicted by the simulation program which results in less than 5% of error. The value that the simulation program predicts is 3.14 μm.

The thermodynamic model predicts the performance degradation as summarized in Table 12.

Table 12: Summary of Simulation Results

	Indicated Efficiency	Volumetric Efficiency	Mass Flow Rate[g/s]	Indicated Work [kW]
Before Testing	0.639	0.716	21.364	1.365
After testing under condition B for 30 days	0.612	0.687	20..4742	1.366

The first row of data shows the predicted performance characteristics of the compressor based on design tolerances. The second row is the predicted performance characteristics of the compressor based on the wear simulation results. As it is shown there is about 4.05% reduction in volumetric efficiency. These results agree with experimental results with about 6.9% of error.

Figure 19 and Figure 20 graphically compare the experimental and simulated results of volumetric efficiency and mass flow rate. As it was mentioned earlier the model does not predict the aging effect which happens in the first few days of the compressor's use. The experimental and simulated results agree within less than 10% of error.

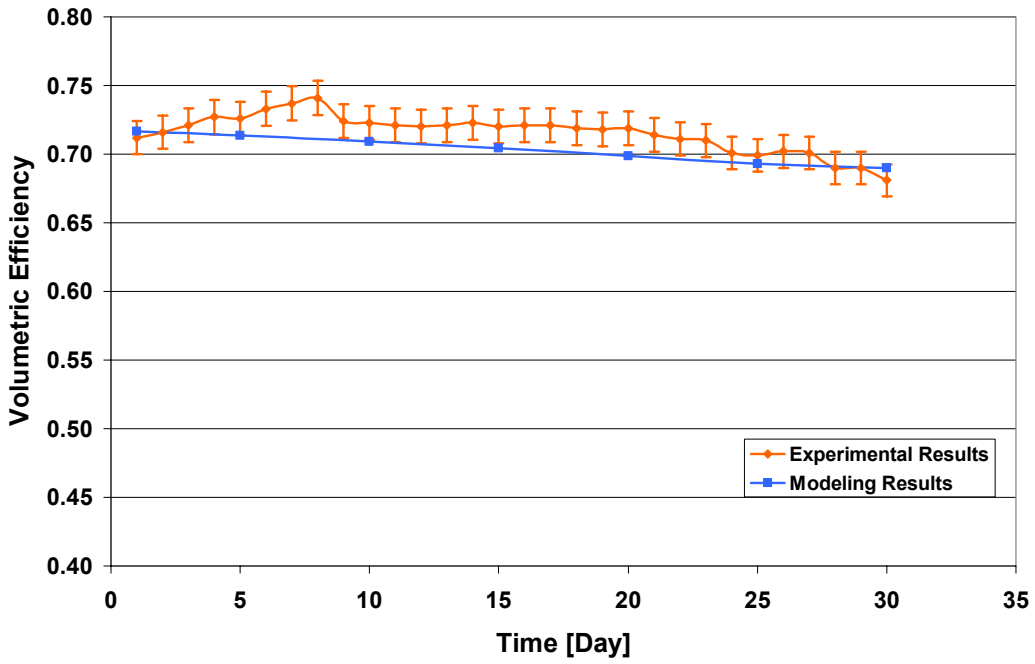

Figure 19: Comparison of Experimental and Simulated Values of Volumetric Efficiency

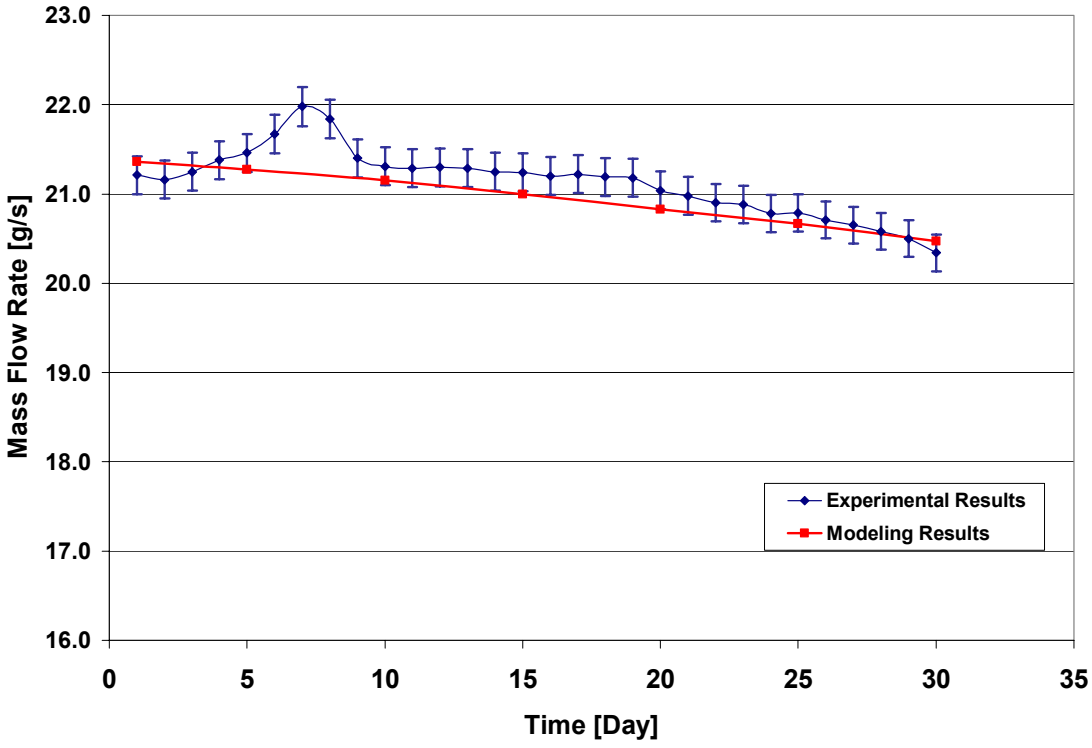

Figure 20: Comparison of Experimental and Simulated Values of Mass Flow Rate

The model was also validated with manufacturer's data which due to confidentiality are not presented here. The model and manufacturer's data agree also within less than 10% of error.

Now that the model has been verified with experimental data, it can be used to predict the life span of compressor at normal use condition (condition D). As shown in Figure 21, the capacity of this particular compressor drops 10% in about 191 days when tested under condition B. While it takes about 650 days to drop by the same amount under normal use condition (condition D).

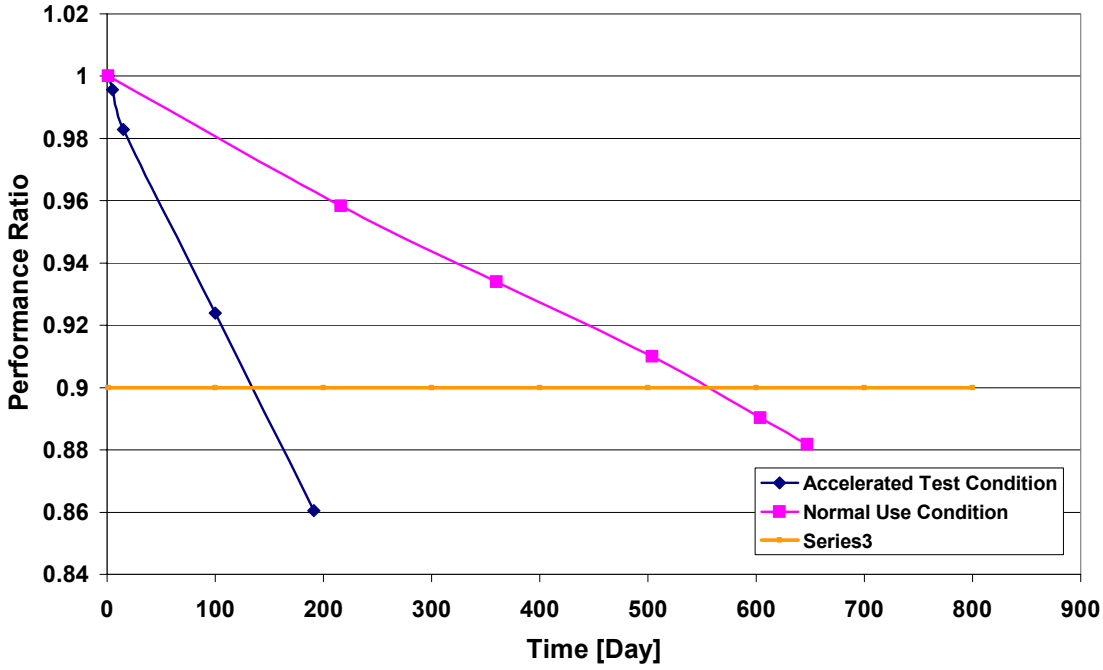

Figure 21: Prediction of Compressor's Life Span under Normal Use Condition

The model can be used to predict the compressor performance under different operating conditions as well.

It is important to notice that the effect of any metal debris contained in the oil/refrigerant mixture due to wear on the vane and roller on the performance of the compressor has not been taken into account. Metal debris may increase the amount of wear on the outer diameter of the rolling piston.

6 Conclusions

As an effort to understand the effect of internal leakage on the performance of rolling piston rotary type compressors, a compressor test facility and a simulation tool was developed.

A bolted case rolling piston rotary type compressor was installed in the constructed test facility. Performance degradation of the compressor was monitored through the test facility over time under a specific test condition. Also the wear development on the rolling piston of the compressor was measured before and after one month of testing.

The simulation tool, predicts the amount of wear on the outer diameter of the rolling piston. As the consequence of wear development the rolling piston/cylinder wall clearance height increases and it results in higher leakage rate from suction pocket to discharge pocket through that specific leak path. As the leakage rate increases, performance of the compressor degrades.

Summary of the obtained results through experiment and modeling is given in Table 13.

Table 13: Comparison of Experimental and Modeling Results

	Experiment	Simulation	Error
Wear on the outer diameter of the rolling piston [μ m]	3	3.14	4.6%
Reduction of volumetric efficiency [%]	4.35	4.05	6.9%

As it was illustrated, internal leakage has a significant effect on the performance reduction of rolling piston rotary type compressors. This method can be used by compressor manufacturers to estimate the life span of this type of compressor under different operation conditions.

In the following section, a list of recommended work of future studies is given. A more general study on the effect leakage through other leak paths on the performance of the compressor would result in a more reliable model.

7 Future Work

Recommended future work as the continuation of this study can is listed below:

- Verify the compressor model at different operation conditions.

- In the compression process major losses occur while the gas is being sucked from the suction valve or being expelled from the discharge valve. In the modeling tool, both valves have been assumed to be ideal. For future work it is suggested to study the effect of pressure losses and time delays in both suction and discharge valve.

- The compressor should be tested for a longer time to be able to compare the experimental results with the modeling results more accurately. Also, the model should be verified experimentally at other operational conditions.

- Performance degradation due to wear on the other parts of the compression compartment such as vane, shaft, bearing, and vane slot should be studied.

8 Uncertainty Analysis

The uncertainty of this experiment was determined using the Pythagorean summation of the discrete uncertainties as shown in Equation 83.

$$u_f = \sqrt{\left(u_{x1} \cdot \frac{\partial f}{\partial x1}\right)^2 + \left(u_{x2} \cdot \frac{\partial f}{\partial x2}\right)^2 + ... + \left(u_{xn} \cdot \frac{\partial f}{\partial xn}\right)^2} \qquad \text{Equation 83}$$

where

u_f: The overall uncertainty of function f resulting from individual uncertainties of $x_i..x_n$

x_i: Nominal values of variables

u_{xi}: Discrete uncertainties

During the experiment several sources of error have been identified which are listed below:

- Pressure Measurements Errors
- Temperature Measurements Errors
- Mass Flow Rate Measurement Error

The uncertainty associated with volumetric efficiency and capacity of the compressor is listed in Table 14.

Table 14: Estimated Uncertainties of Characteristic Parameters

Parameter	Mode	Uncertainties
Volumetric Efficiency	Steady State	± 1.67%
Capacity	Steady State	± 0.5%

9 References

ASHRAE Handbook of HVAC Systems and Equipments, I-P 2000, Compressors, Chapter 34, pp. 34.9-34.11

Bhushan, B., Principles and Applications of Tribology, J. Wiley & Sons, ISBN0-471-59407-5, 1999, chapter 8.

Bird, R., B., Stewart, W., E., Lightfoot, E., N., 2002, Transport Phenomena, 2nd Edition, J. Wiley& Sons, Inc., New York, ISBN 0-471-41077-2, pp. 870-871

Cusano, C., B. Davis. The Tribological Evaluation of Compressor Contacts Lubricated by Oil-Refrigerant Mixtures. Prepared as part of ACRC Project 04, Compressor-Lubrication, Friction, and Wear. 1992

Fujimoto S. Sakitani K., Watada M., "Tribology Analysis in Rolling Piston Type Compressor", Proceedings of the 1984 International Compressor Engineering Conference, Purdue University, West Lafayette, Indiana, 1984

Hamrock, B. J. and Pan, P.: "Simple Formulas for Performance Parameters used in Elastohydrodynamically Lubricated Line Contacts", Journal of Tribology, vol. 111, No. 2, pp.246-251, 1989

Hans-Joachim Huff, Reinhard Radermacher, CO2 Compressor-Expander Analysis, Prepared for the Air-Conditioning and Refrigeration Technology Institute, ARTI-21CR/611-10060-01, March 2003

Huff, H.J., Integrated Compressor-Expander Devices for Carbon Dioxide Vapor Compression Cycles, Ph.D. Thesis, University of Maryland, College Park, 2003

Hutchings, I.M., Tribology: Friction and Wear of Engineering Materials, ISBN 0-8493-7764-1, 1992, chapters 4-5.

Ishiyama A., Iizuka T., Kawashima K., Sekigami K., Hata H, Sugano T., "Study of Technology for refrigerant applications, 2. Lubrication of rotary compressor in HFC-based alternates", Proceedings of the International Compressor Engineering Conference, Purdue University, West Lafayette, Indiana, 1994.

Jenkins S.A., Rotary Compressor Model for Investigating Compressor Performance and Reliability, M.S. Thesis, Massachusetts Institute of Technology, 1998.

Lin Z.H., 1982, Two-Phase Flow Measurement with Sharp Edge Orifices, Int J. Multiphase flow, volume 8, No. 8, pp 683-693, 1982.

McQuiston F., Parker J., Spitler J., Heating, Ventilating, And Air Conditioning, Fifth Edition, 2000, Chapter 15, pp. 532-548.

Preissner M., Carbon Dioxide Vapor Compression Cycle Improvements with Focus on Scroll Expander, Ph.D. Thesis, University of Maryland, College Park, 2001.

Sakaino, K. , et al., Some Approaches Towards a Highe Efficient Rotary Compressor. Proceedings of the International Compressor Engineering Conference, Purdue University, West Lafayette, Ind. 1984.

Sarkar A.D., Friction and Wear, Academic Press Inc., 1980, chapter 3.
Schein, C.S., Development of a Scroll Compressor Computer Model. Masters Thesis, University of Maryland, College Park, 1998.

Sonntag, E., C. Borgnakke, Introduction to Engineering Thermodynamics, J. Wiley& Sons, Inc., New York, ISBN 0-471-32172-9, pp.455 – 477.

Takebayashi, M., H. Kohsokabe, H. Hata, K. Sekigami, Method for Accelerating the Estimation of Wear in Rolling-Piston-Type Rotary Compressors", ASHRAE Trans. 1998, Vol.104, Part 1, 1998.

Wakabayashi, H., J. Yuuda, T. Aizawa, M. Yamamura. Analysis of performance in a rotary compressor. Proceedings of the International Compressor Engineering Conference, Purdue University, West Lafayette, Ind. 1982.

White F.M., Fluid Mechanics, McGraw-Hill Book Company, New York, St. Luis, San Francisco, 1994.

White, F.M., Fluid Mechanics, New York: McGraw-Hill, 1994, 3rd Edition
Yanagiswa T., Shimizu T., Leakage Losses with a Rolling Piston Type Rotary Compressor. I. Radial Clearance on the Rolling Piston, International Journal of Refrigeration, 1985, pp. 75-84.

Yanagiswa T., Shimizu T., Leakage Losses with a Rolling Piston Type Rotary Compressor. II. Radial Clearance on the Rolling Piston, International Journal of Refrigeration, 1982.

Yanagiswa T., T. Shimizu, I. Chu and K Ishijima. Motion Analysis of rolling piston rotary compressor. Proceedings of the International Compressor Engineering Conference, Purdue University, West Lafayette, Ind. 1982